

# A theoretical perspective on mode collapse in variational inference

Roman Soletskyi<sup>1,2</sup>, Marylou Gabri  <sup>1,2</sup>, and Bruno Loureiro<sup>3</sup>

<sup>1</sup>CMAP, CNRS,   cole polytechnique, Institut Polytechnique de Paris, 91120 Palaiseau, France

<sup>2</sup>Laboratoire de Physique de l'  cole normale sup  rieure, ENS, Universit   PSL, CNRS, Sorbonne Universit  ,  
Universit   de Paris F-75005 Paris, France

<sup>3</sup>D  partement d'Informatique,   cole Normale Sup  rieure - PSL & CNRS, France

October 18, 2024

## Abstract

While deep learning has expanded the possibilities for highly expressive variational families, the practical benefits of these tools for variational inference (VI) are often limited by the minimization of the traditional Kullback-Leibler objective, which can yield suboptimal solutions. A major challenge in this context is *mode collapse*: the phenomenon where a model concentrates on a few modes of the target distribution during training, despite being statistically capable of expressing them all. In this work, we carry a theoretical investigation of mode collapse for the gradient flow on Gaussian mixture models. We identify the key low-dimensional statistics characterizing the flow, and derive a closed set of low-dimensional equations governing their evolution. Leveraging this compact description, we show that mode collapse is present even in statistically favorable scenarios, and identify two key mechanisms driving it: mean alignment and vanishing weight. Our theoretical findings are consistent with the implementation of VI using normalizing flows, a class of popular generative models, thereby offering practical insights.

## 1 Introduction

Sampling is a fundamental task in science, arising across a variety of contexts such as machine learning [Teh et al., 2003], Bayesian inference [MacKay, 2002] and statistical physics [Krauth, 2006]. Nevertheless, it can be a challenging problem, and understanding when a target distribution of interest can be efficiently sampled is largely an open question. Variational Inference (VI) addresses this problem by approximating the target distribution  $p$  by minimizing the Kullback-Leibler (KL) divergence  $D_{\text{KL}}(q||p)$  with respect to a conveniently chosen family of tractable distributions  $q \in \mathcal{Q}$ .

A major limitation of VI is the expressiveness of the variational family  $\mathcal{Q}$ . To ensure that  $D_{\text{KL}}(q||p)$  is easy to evaluate, the family  $\mathcal{Q}$  is restricted to distributions with a tractable normalization constant and/or easy to sample from. These requirements often imply turning to factorized distributions (leading to independent covariates) or Gaussian measures which are choices of  $\mathcal{Q}$  that cannot be adequate in all interesting settings. In this context, normalizing flows [Tabak and Vanden-Eijnden, 2010, Papamakarios et al., 2021, Kobyzev et al., 2021] and autoregressive models [Larochelle and Murray, 2011, Uria et al., 2016] - both deep generative models with tractable normalized density and efficient sampling procedures - appear as promising variational families with an increased flexibility upon Gaussian or factorized measures. A series of work have already demonstrated the relevance of these deep learning approaches, both in the context of machine learning [Rezende and Mohamed, 2015] and statistical physics [Wu et al., 2019, Albergo et al., 2019] problems. In the aforementioned examples, the KL divergence is typically minimized using a variation of gradient descent on the neural net parameters.

Despite its popularity, it is well known that VI often encourages a mode-seeking behavior, capturing only one of the (typically) multiple target modes [Regli and Silva, 2018, Jerfel et al., 2021, Blessing et al., 2024]. This phenomenon, known as *mode collapse*, is not resolved by using expressive variational families such as normalizing flows and autoregressive networks despite their ability to represent multi-modal distributions. In this context, solutions to mode collapse have been proposed, including annealing [Wu et al., 2019], adding

a negative likelihood term of approximate samples from  $p$  to the optimized objective [Noé et al., 2019] or dropping the VI objective altogether using an adaptive Monte Carlo framework instead [Gabrié et al., 2022]. Yet, to this date, the mechanisms behind mode collapse remain poorly understood.

In this work, we take a first step towards closing this gap by investigating the dynamics of gradient-based optimization in the simplest setting of a bi-modal Gaussian mixture target distribution  $p$ . Our **main findings** are:

- First, we empirically show that mode collapse is present when learning this simple target model with different choices of variational families  $q \in \mathcal{Q}$ , such as normalizing flows and Gaussian mixtures. We identify two mechanisms, mean alignment and vanishing weights, that drive mode collapse in these experiments.
- Focusing on the simplest example of a Gaussian mixture models, we derive an exact description of the gradient flow dynamics for VI that allow us to study mode collapse in terms of the fixed points of a low-dimensional dynamical system for the relevant summary statistics. Leveraging this description, we mathematically investigate both the mean alignment and weight vanishing mechanisms identified in the experiments.
- Finally, we revisit mode collapse for normalizing flows from the perspective of our analytical findings, showing that they indeed share much of the phenomenology found for well-specified VI. We further investigate how initialization and specific parameterization of the variational distribution might help mitigating mode collapse.

**Related work** — While mode collapse is a well known phenomenon, to the best of our knowledge, there exists very few systematic studies of where and why it arises. Recently, Blessing et al. [2024] conducted a large scale empirical evaluation of VI approaches, reporting that mode collapse becomes harder and harder to avoid as the dimension increases, but without discussing mechanisms driving it.

Conversely, Huix et al. [2024] derived theoretical guarantees on VI through the gradient flow on a mixture of Gaussian with fixed weights, a setting that is considered below, but did not focus on multi-modal target distributions and did not discuss the occurrence of mode collapse.

The loss landscape of Gaussian mixture models has been widely studied, both empirically and theoretically, in the context of maximum likelihood estimation (MLE) and expectation maximization [Srebro, 2007, Jin et al., 2016, Xu et al., 2016, Fan et al., 2023, Chen et al., 2024]. We stress that this is a different problem from the one considered here. While the MLE assumes samples from the target probability are available such that all modes will be covered, in VI one cannot evaluate the target, and therefore resorts to the reverse KL learning objective estimated using exclusively samples from the variational model. In this context, some modes can be completely missed by the model.

Finally, the study of training dynamics through the lenses of a low-dimensional dynamical system for the correlation functions (or summary statistics) is a classical topic in the statistical physics of learning literature [Kinouchi and Caticha, 1992, Saad and Solla, 1995, 1996]. More recently, it has been widely employed in the study of SGD for neural networks [Goldt et al., 2019, Refinetti et al., 2021, Veiga et al., 2023, Ben Arous et al., 2022, 2023, Arnaboldi et al., 2023b,a, 2024, Collins-Woodfin et al., 2023, Patel et al., 2023, Jain et al., 2024, Mori et al., 2024]. However, to our best knowledge this is the first work to use these ideas to the study of VI.

## 2 Mode collapse in variational inference

Consider a target distribution  $p$  on  $\mathbb{R}^d$  that we would like to sample from. Variational inference consists of finding an approximation of  $p$  within a chosen family  $q \in \mathcal{Q}$  of distributions on  $\mathbb{R}^d$  by minimising the Kullback-Leibler (KL) divergence:

$$D_{\text{KL}}(q||p) = \mathbb{E}_q \log q(x) - \mathbb{E}_q \log p(x), \quad (1)$$

where  $\mathbb{E}_\nu$  stands for the expectation with respect to the distribution  $\nu$ . Note that for notational convenience we use the same notation for a distribution and its density with respect to the Lebesgue measure. The

function  $q \mapsto D_{\text{KL}}(q||p)$  is convex and, provided  $p \in \mathcal{Q}$ , it admits a unique minimum for  $q = p$ . However, even in this optimistic scenario optimising in the space of measures is computationally intractable. Therefore, the common practice consists of choosing a parametric family  $\mathcal{Q} = \{q_\theta; \theta \in \Theta\}$  and optimising  $\mathcal{L}(\theta) = D_{\text{KL}}(q_\theta||p)$  over  $\theta \in \Theta$ . Our focus in this work is on the popular case where a Monte Carlo estimator of  $\nabla \mathcal{L}(\theta)$  is available, and optimisation over  $\theta \in \Theta$  is done by a descent-based method.

Note that the VI objective in eq. (1) consists of two terms. The first is the entropy, and favours distributions with lighter tails. On the other hand, the second term vanishes if  $q_\theta = 0$  where  $p > 0$ . Together, this results in a mode-seeking behavior [Regli and Silva, 2018, Miller et al., 2017]: for multi-modal  $p$ , the optimal  $q$  might approximate only a subset of the modes and, as a result, not cover the full  $p$  distribution.<sup>1</sup> As a consequence, VI is prompt to mode collapse. Next section illustrates this discussion on a few preliminary experiments, showing that mode collapse is present even when  $p \in \mathcal{Q}$ .

**Preliminary experiments** — Our starting point is the minimal example of a multi-modal target distribution  $p$ : a mixture of two isotropic Gaussians in dimension  $d = 2$ :

$$p = w_\star \mathcal{N}(\mu_\star, I_2) + (1 - w_\star) \mathcal{N}(-\mu_\star, I_2), \quad (2)$$

where  $\mathcal{N}(\cdot, \cdot)$  stands for the Gaussian distribution,  $\mu_\star$  is a mean vector chosen such that the modes are well-separated and  $w_\star \in (0, 1/2)$  such that the mixture is unbalanced. Figure 1 reports the evolution of the gradient descent dynamics on the VI objective for different classes of  $q_\theta \in \mathcal{Q}$ . While the normalizing flow (NF) can represent the bi-modal target (first column), increasing the distance between target clouds can lead to mode collapse (second column). We simplify further the experiment by considering as  $q_\theta$  a mixture of two Gaussians with the components means and weights as tunable parameters, leaving the covariances equal to identity. Here, we observe that mode collapse is typically the result of one of the components weights going to zero following the alignment of the other component with one of the target’s components (third column). Lastly, we fix the balance of the weights of the variational model to be equal to the balance in the target and run the gradient descent solely on the means. Mode collapse can also happen in this setting with the two means flowing to the same target component (last column).

These preliminary experiments show that mode collapse is present even in the simplest multi-modal VI tasks, and unveils two possible mechanisms behind it: weight vanishing and mean alignment. Normalizing flows do not have a well defined bi-modality as the bi-model Gaussian model but their behavior seems to be closer to the former case: two clouds start to form but in the end only one prevails. Our goal in the following is to develop a mathematical understanding of these two mechanisms for mode collapse in the simpler Gaussian mixture model.

### 3 Variational inference with Gaussian mixtures

In this section, we consider the minimal model for mode collapse discussed in section 2, a mixture of two isotropic Gaussian clouds in  $\mathbb{R}^d$ :

$$\begin{aligned} p(x) &= w_\star \mathcal{N}(x|\mu_\star, I_d) + (1 - w_\star) \mathcal{N}(x|-\mu_\star, I_d), \\ q_\theta(x) &= w_1 \mathcal{N}(x|\mu_1, I_d) + w_2 \mathcal{N}(x|\mu_2, I_d), \end{aligned} \quad (3)$$

with  $w_\star \in (0, 1)$ ,  $w_1 + w_2 = 1$  and without loss of generality we assumed the target means to be symmetric around the origin. Note that although  $p, q_\theta$  belong to the same parametric family, we denote the variational distribution  $q_\theta$  to stress that  $\theta = \{w_1, w_2, \mu_1, \mu_2\} \in \mathbb{R}^{2(d+1)}$  are the trainable parameters. Note that the discussion in this section is readily generalized to a variational family of Gaussian mixtures with more modes, but to simplify the exposition we focus here in the bi-modal case, referring the interested reader to Appendix A for the general case. We denote  $R^2 = \|\mu_\star\|_2^2$  and define for convenience the ratio of target weights  $\gamma := w_\star/(1 - w_\star)$ .

<sup>1</sup>Note that, on the contrary, minimising the direct KL divergence  $D_{\text{KL}}(p||q) \neq D_{\text{KL}}(q||p)$  results in mass-covering behavior. Indeed, if  $q$  does not cover some mode and vanishes where  $p > 0$ , the second term gives an infinite penalty. However, estimating the direct KL divergence requires sampling from  $p$  which is, by construction in VI, computationally hard in practice.

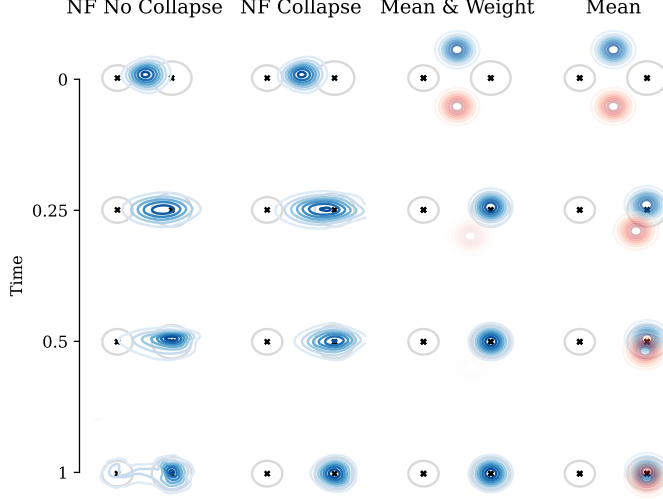


Figure 1: Evolution of gradient descent dynamics from initialization  $T = 0$  to convergence  $T = 1$  for VI on a 2-Gaussian mixture target distribution  $p(x)$  as in eq. (2) with  $\|\mu_\star\|_2 = 2.5$  for the first column,  $\|\mu_\star\|_2 = 3.1$  for the remaining ones, and  $w_\star = 1/3$  for all the columns. The mode position is marked by a black cross, and the 9th decile by gray lines. **(First and second)**  $q_\theta$  depicted in blue is parameterized by a normalizing flow, see appendix B.1. **(Third)**  $q_\theta(x) = w_1\mathcal{N}(\mu_1, I_2) + w_2\mathcal{N}(\mu_2, I_2)$  where we optimize over both means and weights  $\theta = (w_1, w_2, \mu_1, \mu_2)$ . **(Fourth)**  $q_\theta(x) = w_\star\mathcal{N}(\mu_1, I_2) + (1 - w_\star)\mathcal{N}(\mu_2, I_2)$  where we optimize only over the means  $\theta = (\mu_1, \mu_2)$ . In the last two columns the density the different components of  $q_\theta$  are depicted in different colors and their opacity is proportional to their weight.

As discussed in section 2, variational inference consists of minimising the following objective:

$$\min_{\theta} [\mathcal{L}(\theta) := D_{\text{KL}}(q_\theta \| p)]. \quad (4)$$

Our main goal in this section is to investigate the gradient flow dynamics:

$$\dot{\theta} = -\nabla_{\theta} \mathcal{L}. \quad (5)$$

Note that in practice one considers instead gradient descent at small learning rate  $\eta > 0$  and an empirical approximation of the loss function eq. (4) over a large finite batch  $B$  from  $q_\theta$ , which is indeed what is considered in the numerical experiments.

### 3.1 Fixed weight dynamics

The empirical results from section 2 suggest that mode collapse can be driven either by vanishing weights  $w_1, w_2$  or by mean alignment. In order to study these separately, we start our investigation by considering a fixed weight scenario where  $w_1, w_2$  are fixed and only the means are trained. To simplify the analysis further, we fix the norm of the means  $\mu_1, \mu_2 \in \mathbb{S}^{d-1}(R)$  and consider a spherical flow:

$$\dot{\mu}_c = \nabla_{\mu_c}^{\mathbb{S}} \mathcal{L} = \left( I_d - \frac{\mu_c \mu_c^\top}{R^2} \right) \nabla_{\mu_c} \mathcal{L}, \quad c = 1, 2. \quad (6)$$

Although the analysis can be equally carried for standard gradient flow, we have found that the evolution of the norm does not play a major role in the presence (or lack of thereof) of mode collapse, and we refer the interested reader to Appendix A for details on the Euclidean flow. The key idea in our analysis is to notice that mode collapse can be entirely characterized by the evolution of the following three correlations:

$$m_1 = \frac{\mu_1^\top \mu_\star}{R^2}, \quad m_2 = \frac{\mu_2^\top \mu_\star}{R^2}, \quad s = \frac{\mu_1^\top \mu_2}{R^2} \quad (7)$$

This allows us to reduce the high-dimensional evolution of means  $\mu_1, \mu_2 \in \mathbb{S}^{d-1}(R)$  in eq. (6) to a low-dimensional evolution in terms of sufficient statistics  $m_1, m_2, s \in [-1, 1]$ :

$$\begin{aligned}\dot{m}_1 &= -[(m_2 - m_1 s)f(s) + w_1(1 - m_1^2)g(m_1)] \\ \dot{m}_2 &= -[(m_1 - m_2 s)f(s) + w_2(1 - m_2^2)g(m_2)] \\ \dot{s} &= -[2(1 - s^2)f(s) + w_1(m_2 - m_1 s)g(m_1) + w_2(m_1 - m_2 s)g(m_2)]\end{aligned}\quad (8)$$

where the auxiliary functions  $f, g : [-1, 1] \rightarrow \mathbb{R}$  are given by:

$$\begin{aligned}f(s) &= \mathbb{E}_z \left[ w_1 \sigma \left( R^2(s-1) + zR\sqrt{2(1-s)} - \log \frac{w_1}{w_2} \right)^2 + w_2 \sigma \left( R^2(s-1) + zR\sqrt{2(1-s)} + \log \frac{w_1}{w_2} \right)^2 \right] \\ g(m) &= 1 - 2\mathbb{E}_z \left[ \sigma \left( 2R^2 m + 2Rz + \log \frac{w_\star}{1 - w_\star} \right) \right]\end{aligned}\quad (9)$$

with  $z \sim \mathcal{N}(0, 1)$  and  $\sigma(t) := (1 + e^{-t})^{-1}$  denote the sigmoid function. Note that  $g$  is a monotonic function. The detailed derivation can be found in Appendix A.2.

### 3.1.1 Fixed points of the dynamics

Since eq. (6) is a descent algorithm, it converges to zero gradient points of  $\mathcal{L}$  (provided they exist). The low-dimensional equations eq. (8) provide a convenient way of classifying these fixed points and detecting mode collapse. In the following, we will say the dynamics has mode collapsed if it converges to a fixed point  $(m_1^*, m_2^*, s^*)$  such that  $s^* > 0$ .

Consider the case where the weights of the variational distribution are fixed to their optimal value  $w_1 = (1 - w_2) = w_\star$ . This is a statistically favorable scenario where the variational model is well-specified, initialized with the correct target weights and norm  $R$ . Yet, as we will see now, mode collapse is still present. More precisely, in Appendix A.3 we prove that eq. (8) has three types of fixed points:

- (i) **Global minimum and flipped fixed point:** The global minima of the loss is given by  $\mu_1 = -\mu_2 = \mu_\star$  which corresponds to  $(m_1^*, m_2^*, s^*) = (1, -1, -1)$ . Flipping the role of  $\mu_1$  and  $\mu_2$  yields another fixed point of eq. (8),  $(m_1^*, m_2^*, s^*) = (-1, 1, -1)$ , which is also a global minima of the loss in the symmetric case  $w_\star = 0.5$ .
- (ii) **Perfect alignment mode collapse:** Corresponds to  $\mu_1 = \mu_2$  and hence to  $s^* = 1$ . This is a fixed point of eq. (8) provided  $m_1^* = m_2^* = m$  and  $m = \pm 1$  or  $g(m) = 0$ . Since  $g$  is monotonic in  $[-1, 1]$ , it has a unique root. Hence, there are 3 perfect alignment fixed points.
- (iii) **Other fixed points:** Other fix points exists with  $m_1^* \neq m_2^*$  and  $s^* \neq 1$ , but a closed-form expression is not available. Nevertheless, they can be easily studied numerically by computing zeroes of eq. (8) over  $(m_1, m_2, s) \in (-1, 1)^3$ . In particular, mean alignment mode collapse corresponds to fixed points where  $s^* \in (0, 1)$ .

To determine whether a fix point  $(m_1^*, m_2^*, s^*) \in [-1, 1]^3$  is an attractor or repeller of the flow, we must study the spectrum of the Hessian at the fixed point. In particular, if the smallest eigenvalue is positive, the fixed point is attractive/stable, and corresponds to a minimum of the loss.

Remarkably, the eigenvalues of the Hessian can be explicitly computed for the scenarios (i), (ii) discussed above - see Appendix A.3. In these cases, we can show that the only stable fixed points are the global minimum and above a certain  $R$  and flipped fixed points, both corresponding to a non-collapsed outcome with  $s^* = -1$ . The perfect alignment mode collapse fixed points  $s^* = 1$  instead are always unstable.

Searching for other fixed points with  $s^* \neq 1$ , one finds numerically that below a certain critical threshold  $R < R_c$ , (i), (ii) are the only fixed points of the flow eq. (8). This means that for small radius, the mode collapse fixed point is always unstable, and hence not reached dynamically.

On the other hand, above the critical threshold  $R > R_c$  an additional fixed point with  $s^* \in (0, 1)$  appears. One can check numerically that this mean alignment mode collapse fixed point is stable. Interestingly, despite being stable this fixed point is not universally attracting in the  $(m_1, m_2, s)$ -plane, meaning that whether the

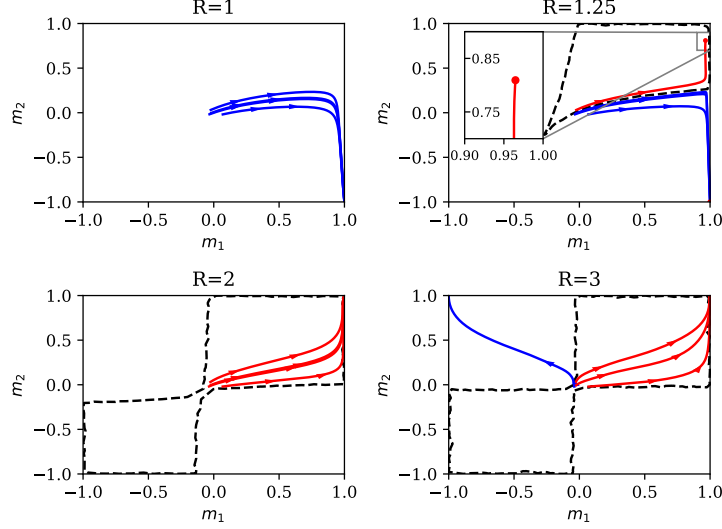


Figure 2: Basin of attraction of the mean alignment fixed points  $m_1 = m_2 = \pm 1$  on the  $s = 0$  cross section of phase space  $(m_1, m_2, s) \in [-1, 1]^3$  for  $R \in \{1, 1.25, 2, 3\}$ ,  $d = 1000$ ,  $w_* = 2/3$ , and  $\eta = 0.05$ . The dashed black line denote the boundary of the basin of attraction of the mode collapse fixed points. Solid lines denote individual flow trajectories with different random initialization  $\mu_1, \mu_2 \sim \text{Unif}(\mathbb{S}^{d-1}(R))$ . Mode collapsed trajectories are red, avoiding it are blue.

flow in eq. (8) converges to it or to the global or flipped minimum, thereby avoiding mode collapse, depends on the initialization of the means  $\mu_1, \mu_2$ . To lead further the discussion, we consider next the high-dimensional scenario where the initialization of the summary statistics likely lies close to the origin.

### 3.1.2 High-dimensional scenario

Typically, the VI practitioner has no information on the ground truth means  $\mu_*$ , and therefore initializes the algorithm independently at random  $\mu_1, \mu_2 \sim \text{Uni}(\mathbb{S}^{d-1}(R))$ . Therefore, with high-probability one has  $m_1, m_2, s = O(1/\sqrt{d})$  at initialization.

In fig. 2, we illustrate the typical trajectories of the summary statistics in the plane  $(m_1, m_2)$  for uniformly random initialization of the means on the  $d$ -dimensional sphere and increasing values of the radius  $R$ . Consistently with the above stability analysis, below  $R_c$  the dynamics converge to the global minimum. For  $R > R_c$ , the outcome depends on initialization even in this high-dimensional scenario.

For  $R > R_c$ , we investigate numerically the basin of attraction of the mode collapse stable fixed points, that is with  $s^* \in (0, 1)$  (scenario (iii)). The dashed black line represents the boundary of their basin of attraction at a  $s = 0$  slice of the phase space  $(m_1, m_2, s)$ : under the flow eq. (6), any initial condition  $(m_1^0, m_2^0, 0)$  inside this region necessarily flows to the mode collapse mean alignment fixed point. Interestingly, the boundaries of the basin attraction lies very close to the origin for some directions meaning that fluctuations can lead to initialization outside the basin, even in high-dimension. Whether a trajectory will converge to the global or flipped minimum or mode collapse therefore crucially depends on the initialization even at large  $d$ . Moreover, fig. 2 suggests that for large  $R$ , the basin of attraction of mode collapse consists of the symmetric quadrants  $m_1 m_2 > 0$ . This behavior can be mathematically understood by noting that  $f(s)$  in eq. (9) is  $O(e^{-2(1-s)R^2})$  when  $s < 1$ . Hence, assuming  $s$  remains smaller than 1,  $f(s)$  is exponentially small along the flow trajectory, and the evolution of  $(m_1, m_2)$  is approximately autonomous:

$$\dot{m}_{1,2} \approx -w_{1,2}(1 - m_{1,2}^2)g(m_{1,2}). \quad (10)$$

Since  $g$  is a decreasing function, once  $|m|$  starts to increase, it monotonically continues along the entire trajectory. Therefore, for  $R$  large enough, the final value of  $m$  is completely determined by the sign of  $g(m)$  at initialization. Note that the sign of  $g(m)$  only changes in a  $O(1/R^2)$  neighborhood of  $m = 0$ . Since under

random initialization  $m^0 = O(1/\sqrt{d})$  with high-probability, when  $1/R^2 \lesssim 1/\sqrt{d} \Rightarrow d \lesssim R^4$ , there is a finite probability that at initialization  $g(m_{1,2})$  have different signs and mode collapse is avoided.

Therefore, in this context a simple strategy to avoid mean alignment mode collapse for systems with moderate dimensions  $d$  is to restart the training with another random seed.

### 3.2 Training the weights

In the previous section, we discussed how mode collapse can dynamically arise even in the statistically favorable scenario where the weights are fixed at their target optimal values, driven by an attractive mean alignment mechanism. In this section, we investigate how training the variational model weights  $(w_1, w_2)$  impacts this discussion.

First, note that the naive flow in eq. (5) does not preserve the normalization of the weights  $w_1 + w_2 = 1$ . Different ways of incorporating this constraint in the flow will lead to different optimization algorithms, which might be more or less prompt to mode collapse. In this manuscript, we focus on the following reparametrization of the weights:

$$w_1 = \frac{v_1}{v_1 + v_2}, \quad w_2 = \frac{v_2}{v_1 + v_2}; \quad (11)$$

for positive  $v_1, v_2 \in \mathbb{R}_+$ . In Appendix A.4, we show that this parametrization for the weights lead to the following normalization preserving flow on the weights:

$$\dot{w}_1 = -(w_1^2 + w_2^2) \left( \frac{\partial \mathcal{L}}{\partial w_1} - \frac{\partial \mathcal{L}}{\partial w_2} \right), \quad \dot{w}_2 = -\dot{w}_1 \quad (12)$$

where

$$\begin{aligned} \frac{\partial \mathcal{L}}{\partial w_1} = & \mathbb{E} \left[ \sigma \left( R^2(1-s) + zR\sqrt{2(1-s)} + \log \frac{w_1}{w_2} \right) \right] + \frac{w_2}{w_1} \mathbb{E} \left[ \sigma \left( -R^2(1-s) + zR\sqrt{2(1-s)} + \log \frac{w_1}{w_2} \right) \right] \\ & - \mathbb{E} \left[ \log \sigma \left( R^2(1-s) + zR\sqrt{2(1-s)} + \log \frac{w_1}{w_2} \right) \right] + \mathbb{E} \left[ \log \sigma \left( 2R^2 m_1 + 2Rz + \log \frac{w_\star}{1-w_\star} \right) \right] \\ & + \log \frac{w_1}{w_\star} + R^2(1-m_1) \end{aligned} \quad (13)$$

where the expectations are over  $z \sim \mathcal{N}(0, 1)$ . A similar expression for the derivative with respect to  $w_2$  is obtained by noting that  $w_2 = 1 - w_1$ . Therefore, the dependence on the means  $\mu_1, \mu_2$  in the flow on the weights in eq. (12) is also entirely captured by the correlation functions  $(m_1, m_2, s)$ .

In the Appendix A.4.2 we also discuss an alternative descent algorithm that projects the weights in the constraint  $w_1 + w_2 = 1$  at every step. In particular, we observe that this projective procedure is more prompt to weight vanishing mode collapse than the reparametrization in eq. (12), highlighting the importance of the implicit algorithmic bias to mode collapse in VI.

**Quasi-mode collapse** — As we saw in the fixed weight dynamics, the existence of stable mode collapse fixed points depend on the distance between target means  $R$ . We start our discussion by numerically observing that a similar phenomenology arises when training the weights. Figure 3 shows the evolution of the correlation functions  $(m_1, m_2, s)$  (top) and weights  $(w_1, w_2)$  under the flow eq. (12), for increasing radii  $R$ . Again, we numerically observe the existence of a critical separation  $R_c$  above which  $s \in (0, 1]$  is a fixed point of the flow, signaling the presence of mode collapse. Note, however, that the mechanism leading to mode collapse is very different and shows its signature even for  $R < R_c$ : early in the dynamics both the means  $\mu_{1,2}$  positively correlates with the same target mode. Once, one of them reaches full alignment with this target modes, the opposite weight starts to decrease, and the evolution of the corresponding mean slows down. This can be understood from the fact that the loss terms in the evolution of the means are proportional to the weight, see eq. (9). For small enough radius  $R$  (fig. 3 left), the small weight eventually recovers, and the dynamics quickly converge to the global minima. However, as the radius is increased (fig. 3 middle), the slow dynamics becomes longer, meaning the system is trapped in an increasingly longer transient state with vanishing weight. We

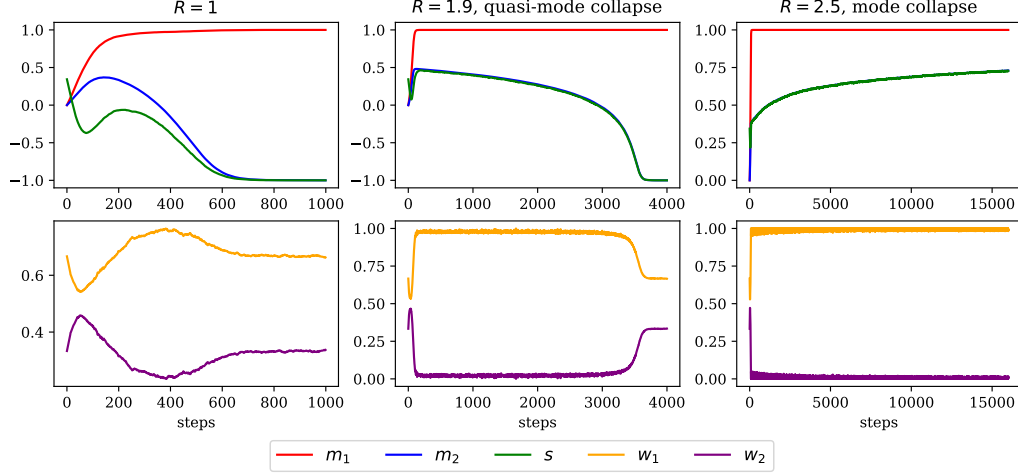


Figure 3: Numerical evolution of sufficient statistics and weights for different radii  $R \in \{1, 1.9, 2.5\}$ . Quasi-mode collapse happens in the middle. Learning rate  $\eta = 0.05$ , batch size  $B = 1000$ ,  $d = 10$  and  $w_\star = 2/3$ .

refer to this phenomena as *quasi-mode collapse*. Finally, above  $R > R_c$  this weight-vanishing mode collapse becomes attractive (fig. 3 right).

We now investigate this empirical observation through the lenses of the summary statistics. First, note that  $\mu_1$  becomes quickly aligned with  $\mu_\star$ , then  $m_1 \approx 1$  and from the problem's geometry  $m_2 \approx s$ . Therefore, the flow of sufficient statistics and weights becomes effectively reduced to the flow of two variables  $(s, w)$  where we have defined  $w$  as smaller weight  $w_2$ . Inserting  $m_1 = 1, m_2 = s$  into eq. (8) and expanding in  $w \ll 1$  in eq. (12) we obtain:

$$\dot{w} = \frac{\partial \mathcal{L}}{\partial w_1} - \frac{\partial \mathcal{L}}{\partial w_2} \quad (14)$$

$$\dot{s} = -(1 - s^2)(2f(s) + wg(s)) \quad (15)$$

Again, from our empirical observation, the evolution of  $s$  is much slower than the evolution of  $w$ . Thus, we can treat  $w$  as fast mode that thermalizes quickly and  $s$  as a slow mode. Then, for most of the trajectory  $w$  can be approximated by its equilibrium value  $w_{\text{eq}}(s)$  which slowly changes with  $s$ . We can find  $w_{\text{eq}}$  by solving the stationary flow equation  $\dot{w} = 0$  at large  $R$ . Consider the following *ansatz* for the expansion  $w$  at large  $R$ :

$$\log w_{\text{eq}} = aR^2 + bR + \dots \quad (16)$$

The coefficients  $a, b$  can be determined by inserting this *ansatz* in the flow equation and approximating  $\log \sigma(x) = -\text{relu}(-x)$  at large  $|x|$ . As a result, we find that when  $s < 0$ , up to a constant:

$$\log w_{\text{eq}} = -R^2(1 + s). \quad (17)$$

This allow us to compute  $f(s)$  at large  $R$ . Using Laplace method, one finds  $f(s) \propto e^{-R^2/(1-s)}$ . Therefore, when  $s > 0$ ,  $g(s) \approx 1$  at sufficiently large  $R$ . Inserting this in eq. (15), we obtain the following approximate dynamics for  $s$ :

$$\dot{s} = -e^{-R^2(1-s)} \quad (18)$$

which admits a closed-form solution  $s = -1 + 1/R^2 \log(e^{R^2} - t)$ . This give us an estimation of the time scale over which the flow stays in a quasi-mode collapse state before recovering  $T_{\text{quasi}} = O(e^{R^2})$ .

Note that the simplification above, concerning the separation between fast  $w$  and slow  $s$  modes, holds for the flow at large radius. However, when comparing with numerical experiments we have observed that the

fluctuations induced by a finite learning rate  $\eta > 0$  in the discretization of the flow can become relevant to the picture. Analyzing this interplay is beyond the scope of the present work, and is an interesting avenue for future work.

## 4 Numerical experiments

Section 3 provided some understanding of the mechanisms behind mode collapse when performing VI using gradient descent. In this last section, we compare the theoretical findings obtained on Gaussian mixtures with the practical case of using NFs for VI on a multi-modal target distribution.

**Experimental setup** — The target distribution  $p$  is kept to be equal to the bimodal Gaussian mixture considered in section 3 in dimension  $d$ . Without loss of generality, we consider the target means to be  $\mu_\star = (R, 0, \dots, 0)$  and  $-\mu_\star$ .

The variational model considered here is a NF of RealNVP-type [Dinh et al., 2017]:  $q_\theta$  is the pushforward of a base distribution  $p_z$  by a diffeomorphism  $f_\theta$ , carrying the parameters  $\theta$  of the VI. The probability density is explicitly given by the change of variable formula

$$q_\theta(x) = p_z(f_\theta^{-1}(x)) |\nabla_x f_\theta^{-1}| \quad (19)$$

where the building blocks of the RealNVP map  $f_\theta$ , called coupling layers, are designed to allow for easy computation of Jacobians. The reverse KL is minimized by stochastic gradient descent on  $\theta$  leveraging an unbiased Monte Carlo estimator of  $\nabla \mathcal{L}(\theta)$  using a batch of size  $B$  of samples from the base distribution  $p_z$ . Details on the architecture and loss computation are deferred to appendix B.

In the experiments below,  $f_\theta$  is initialized close to the identity, such that at the beginning of the learning  $q_\theta \approx p_z$ . Thus we can investigate different strategy of initialization by considering different base distributions: the *centered* case where  $p_z = \mathcal{N}(0, I_d)$ ; the *shifted* case  $p_z = \mathcal{N}(\mu, I_d)$  with  $\mu$  a random vector with norm  $R^2$  and finally the *multi-modal prior* case

$$p_z = w_\star \mathcal{N}(\mu, I) + (1 - w_\star) \mathcal{N}(-\mu, I) \quad (20)$$

where  $\mu$  is again a random vector with norm  $R$ . The latter case closely resembling the fixed weight setting studied in section 3.1, at least at initialization.

To describe the mode collapse phenomenon for NFs, we partition  $\mathbb{R}^d$  into two half-spaces  $H_\pm$  according to the sign of the first coordinate and define the statistics

$$w_\pm = \mathbb{E}_{q_\theta} [\mathbf{1}_{x \in H_\pm}] , \quad (21)$$

$$\mu_\pm = \frac{1}{w_\pm} \mathbb{E}_{q_\theta} [x \mathbf{1}_{x \in H_\pm}] , \quad (22)$$

along with the projections  $m_\pm = \mu_\pm^\top \mu_\star$  and  $s = \mu_+^\top \mu_-$ . In the experiments below, we consider that mode collapse has occurred when at the end of the optimization  $s > 0$  or one of  $w_\pm < 0.01$ .

As a reference, we also report here on the Gaussian mixture setup of section 3.2 initializing means as random vectors  $\mu_{1,2} \sim \text{Unif}(\mathbb{S}^{d-1}(R))$  and weights as  $w_1 = w_\star$  and  $w_2 = 1 - w_\star$ . As above, we consider that mode collapse has occurred when at the end of the optimization  $s > 0$  or one of  $w_{1,2} < 0.01$ .

**Results** — We find that the observation made on Gaussian mixtures that mode collapse occurs when the radius  $R$  is larger than a threshold  $R_c$  is also generally true for NFs. To further quantify this agreement, we perform a binary search on the radius to locate the threshold  $R_c$  as a function of the dimension  $d$ . The binary search is stopped when a tolerance of 0.01 is reached. Since mode collapse can depend on the random initialization, each experiment is repeated with 10 different seeds. The resulting thresholds for NFs with the 3 different priors and the mixture of Gaussian variational family are plotted on fig. 4.

<sup>2</sup>This setup is closer to the Gaussian mixture theory because at initialization the center of the Gaussian cloud approximately lies at the sphere of radius  $R$ .

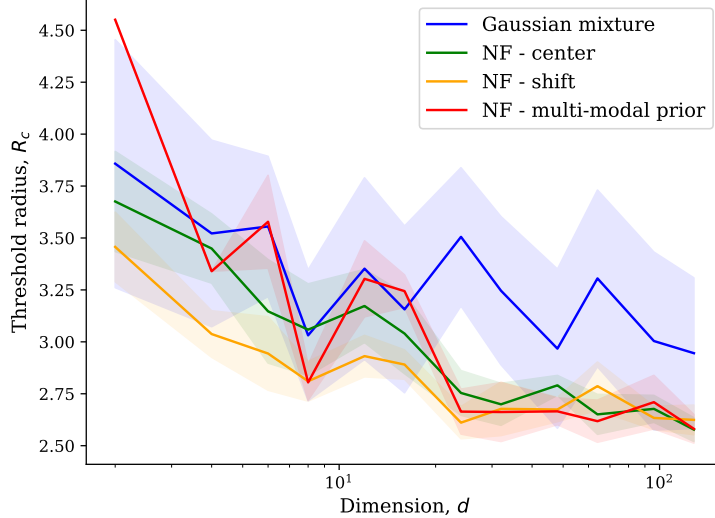


Figure 4: Dependence of threshold radius  $R_c$  on dimension  $d$  for different setups

Interestingly, for the multi-modal prior, we observe that for all tried dimensions  $d$ , up to  $d = 128$ , there are seeds that avoid mode collapse at all  $R$ . For this settings, the radius plotted on section 3.2 only includes seeds that do experience mode collapse. Therefore, the multi-modal prior setup can be beneficial to avoid mode collapse at the cost of having to restart the experiment with a different seed. This observation is consistent with the discussion on Gaussian mixtures with fixed weights of section 3.1.2, such that we expect it to hold at least for moderate dimensions  $d$ .

For the two other NF settings, the threshold  $R_c$  are very similar, especially in large dimension. The Gaussian mixture model enjoys a slightly larger threshold but the qualitative picture is consistent with the NFs:  $R_c$  has a finite value that decreases as  $d \rightarrow \infty$ . This is another indicator of the similarity between the mechanisms behind mode collapse for the Gaussian mixture variational family and the NFs.

## 5 Conclusion

In this work, we have presented a theoretical investigation of mode collapse in variational inference, focusing on the gradient flow dynamics in Gaussian mixture models. Our results build on an exact characterization of the flow in terms of low-dimensional summary statistics. This reduced description maps the study of mode collapse to the study of the fixed points of this low-dimensional dynamical system.

Leveraging this description, we identified two principal mechanisms behind mode collapse: mean alignment and vanishing weights. These mechanisms were shown to drive the collapse even in scenarios where the variational family is statistically well-specified, corroborating the observation that mode collapse is not a by-product of insufficient model expressivity, but a consequence of the optimization procedure.

Additionally, the separation between modes was shown to play a crucial role in determining whether or not mode collapse occurs. This observation was found to be consistent when considering the more powerful variational family of normalizing flows.

The observation that expressivity is not a driving factor of mode collapse suggests that the investigation of mathematically tractable multi-modal variational families, such as the Gaussian mixture model studied here, offers a promising road map towards understanding, and hence mitigating, mode collapse in more complex tasks. The qualitative agreement we observed between theoretical predictions and numerical experiments on more sophisticated models further confirm the relevance of this approach. Our results lay the groundwork in this direction.

## Acknowledgements

We would like to thank Louis Grenioux and Zhou Fan for stimulating discussions. BL acknowledges funding from the *Choose France - CNRS AI Rising Talents* program. MG and RS acknowledge funding from Hi! Paris.

## References

- M. S. Albergo, G. Kanwar, and P. E. Shanahan. Flow-based generative models for Markov chain Monte Carlo in lattice field theory. *Physical Review D*, 100(3):034515, August 2019. ISSN 2470-0010, 2470-0029. doi: 10.1103/PhysRevD.100.034515.
- Luca Arnaboldi, Florent Krzakala, Bruno Loureiro, and Ludovic Stephan. Escaping mediocrity: how two-layer networks learn hard generalized linear models with sgd. *arXiv preprint arXiv:2305.18502*, 2023a.
- Luca Arnaboldi, Ludovic Stephan, Florent Krzakala, and Bruno Loureiro. From high-dimensional & mean-field dynamics to dimensionless odes: A unifying approach to sgd in two-layers networks. In *The Thirty Sixth Annual Conference on Learning Theory*, pages 1199–1227. PMLR, 2023b.
- Luca Arnaboldi, Yatin Dandi, Florent Krzakala, Bruno Loureiro, Luca Pesce, and Ludovic Stephan. Online learning and information exponents: The importance of batch size & Time/Complexity tradeoffs. In Ruslan Salakhutdinov, Zico Kolter, Katherine Heller, Adrian Weller, Nuria Oliver, Jonathan Scarlett, and Felix Berkenkamp, editors, *Proceedings of the 41st International Conference on Machine Learning*, volume 235 of *Proceedings of Machine Learning Research*, pages 1730–1762. PMLR, 21–27 Jul 2024. URL <https://proceedings.mlr.press/v235/arnaboldi24a.html>.
- Gerard Ben Arous, Reza Gheissari, and Aukosh Jagannath. High-dimensional limit theorems for sgd: Effective dynamics and critical scaling. *Advances in Neural Information Processing Systems*, 35:25349–25362, 2022.
- Gerard Ben Arous, Reza Gheissari, Jiaoyang Huang, and Aukosh Jagannath. High-dimensional sgd aligns with emerging outlier eigenspaces. *arXiv preprint arXiv:2310.03010*, 2023.
- Denis Blessing, Xiaogang Jia, Johannes Esslinger, Francisco Vargas, and Gerhard Neumann. Beyond elbos: A large-scale evaluation of variational methods for sampling, 2024. URL <https://arxiv.org/abs/2406.07423>.
- Yudong Chen, Dogyoon Song, Xumei Xi, and Yuqian Zhang. Local minima structures in gaussian mixture models. *IEEE Transactions on Information Theory*, 2024.
- Elizabeth Collins-Woodfin, Courtney Paquette, Elliot Paquette, and Inbar Seroussi. Hitting the high-dimensional notes: An ode for sgd learning dynamics on glms and multi-index models. *arXiv preprint arXiv:2308.08977*, 2023.
- Laurent Dinh, Jascha Sohl-Dickstein, and Samy Bengio. Density estimation using real nvp, 2017.
- Zhou Fan, Yi Sun, Tianhao Wang, and Yihong Wu. Likelihood landscape and maximum likelihood estimation for the discrete orbit recovery model. *Communications on Pure and Applied Mathematics*, 76(6):1208–1302, 2023. doi: <https://doi.org/10.1002/cpa.22032>. URL <https://onlinelibrary.wiley.com/doi/abs/10.1002/cpa.22032>.
- Marylou Gabri , Grant M. Rotskoff, and Eric Vanden-Eijnden. Adaptive Monte Carlo augmented with normalizing flows. *Proceedings of the National Academy of Sciences*, 119(10):e2109420119, March 2022. ISSN 0027-8424, 1091-6490. doi: 10.1073/pnas.2109420119. URL <http://arxiv.org/abs/2105.12603>. arXiv:2105.12603 [cond-mat, physics:physics].
- Sebastian Goldt, Madhu Advani, Andrew M Saxe, Florent Krzakala, and Lenka Zdeborov . Dynamics of stochastic gradient descent for two-layer neural networks in the teacher-student setup. In H. Wallach, H. Larochelle, A. Beygelzimer, F. d’Alch -Buc, E. Fox, and R. Garnett, editors, *Advances in Neural Information Processing Systems*, volume 32. Curran Associates, Inc., 2019.

- Tom Huix, Anna Korba, Alain Oliviero Durmus, and Eric Moulines. Theoretical guarantees for variational inference with fixed-variance mixture of Gaussians. In Ruslan Salakhutdinov, Zico Kolter, Katherine Heller, Adrian Weller, Nuria Oliver, Jonathan Scarlett, and Felix Berkenkamp, editors, *Proceedings of the 41st International Conference on Machine Learning*, volume 235 of *Proceedings of Machine Learning Research*, pages 20700–20721. PMLR, 21–27 Jul 2024. URL <https://proceedings.mlr.press/v235/huix24a.html>.
- Anchit Jain, Rozhin Nobahari, Aristide Baratin, and Stefano Sarao Mannelli. Bias in motion: Theoretical insights into the dynamics of bias in sgd training. *arXiv preprint arXiv:2405.18296*, 2024.
- Ghassen Jerfel, Serena Wang, Clara Wong-Fannjiang, Katherine A. Heller, Yian Ma, and Michael I. Jordan. Variational refinement for importance sampling using the forward Kullback-Leibler divergence. In *Proceedings of the Thirty-Seventh Conference on Uncertainty in Artificial Intelligence*, pages 1819–1829. PMLR, December 2021. URL <https://proceedings.mlr.press/v161/jerfel21a.html>. ISSN: 2640-3498.
- Chi Jin, Yuchen Zhang, Sivaraman Balakrishnan, Martin J Wainwright, and Michael I Jordan. Local maxima in the likelihood of gaussian mixture models: Structural results and algorithmic consequences. In D. Lee, M. Sugiyama, U. Luxburg, I. Guyon, and R. Garnett, editors, *Advances in Neural Information Processing Systems*, volume 29. Curran Associates, Inc., 2016. URL [https://proceedings.neurips.cc/paper\\_files/paper/2016/file/3875115bacc48cca24ac51ee4b0e7975-Paper.pdf](https://proceedings.neurips.cc/paper_files/paper/2016/file/3875115bacc48cca24ac51ee4b0e7975-Paper.pdf).
- O Kinouchi and N Caticha. Optimal generalization in perceptions. *Journal of Physics A: Mathematical and General*, 25(23):6243, dec 1992. doi: 10.1088/0305-4470/25/23/020. URL <https://dx.doi.org/10.1088/0305-4470/25/23/020>.
- Ivan Kobyzev, Simon J.D. Prince, and Marcus A. Brubaker. Normalizing Flows: An Introduction and Review of Current Methods. *IEEE Transactions on Pattern Analysis and Machine Intelligence*, 43(11):3964–3979, November 2021. ISSN 0162-8828, 2160-9292, 1939-3539. doi: 10.1109/TPAMI.2020.2992934.
- Werner Krauth. Statistical mechanics: Algorithms and computations. *OUP Oxford*, 13, 2006.
- Hugo Larochelle and Iain Murray. The Neural Autoregressive Distribution Estimator. In *Proceedings of the Fourteenth International Conference on Artificial Intelligence and Statistics*, pages 29–37. JMLR Workshop and Conference Proceedings, June 2011.
- David J. C. MacKay. *Information Theory, Inference & Learning Algorithms*. Cambridge University Press, USA, 2002. ISBN 0521642981.
- Andrew C. Miller, Nicholas Foti, and Ryan P. Adams. Variational boosting: Iteratively refining posterior approximations, 2017.
- Francesco Mori, Stefano Sarao Mannelli, and Francesca Mignacco. Optimal protocols for continual learning via statistical physics and control theory. *arXiv preprint arXiv:2409.18061*, 2024.
- Frank Noé, Simon Olsson, Jonas Köhler, and Hao Wu. Boltzmann generators: Sampling equilibrium states of many-body systems with deep learning. *Science*, 365(6457):eaaw1147, September 2019. ISSN 0036-8075, 1095-9203. doi: 10.1126/science.aaw1147.
- George Papamakarios, Eric Nalisnick, Danilo Jimenez Rezende, Shakir Mohamed, and Balaji Lakshminarayanan. Normalizing Flows for Probabilistic Modeling and Inference. *Journal of Machine Learning Research*, 22(57):1–64, 2021. ISSN 1533-7928.
- Nishil Patel, Sebastian Lee, Stefano Sarao Mannelli, Sebastian Goldt, and Andrew Saxe. The rl perceptron: generalisation dynamics of policy learning in high dimensions. *arXiv preprint arXiv:2306.10404*, 2023.
- Maria Refinetti, Sebastian Goldt, Florent Krzakala, and Lenka Zdeborova. Classifying high-dimensional gaussian mixtures: Where kernel methods fail and neural networks succeed. In Marina Meila and Tong Zhang, editors, *Proceedings of the 38th International Conference on Machine Learning*, volume 139 of *Proceedings of Machine Learning Research*, pages 8936–8947. PMLR, 18–24 Jul 2021.

- Jean-Baptiste Regli and Ricardo Silva. Alpha-beta divergence for variational inference, 2018.
- Danilo Rezende and Shakir Mohamed. Variational Inference with Normalizing Flows. In *Proceedings of the 32nd International Conference on Machine Learning*, pages 1530–1538. PMLR, June 2015.
- David Saad and Sara Solla. Dynamics of on-line gradient descent learning for multilayer neural networks. In D. Touretzky, M. C. Mozer, and M. Hasselmo, editors, *Advances in Neural Information Processing Systems*, volume 8. MIT Press, 1996.
- David Saad and Sara A. Solla. On-line learning in soft committee machines. *Phys. Rev. E*, 52:4225–4243, Oct 1995. doi: 10.1103/PhysRevE.52.4225. URL <https://link.aps.org/doi/10.1103/PhysRevE.52.4225>.
- Nathan Srebro. Are there local maxima in the infinite-sample likelihood of gaussian mixture estimation? In Nader H. Bshouty and Claudio Gentile, editors, *Learning Theory*, pages 628–629, Berlin, Heidelberg, 2007. Springer Berlin Heidelberg. ISBN 978-3-540-72927-3.
- Esteban G. Tabak and Eric Vanden-Eijnden. Density estimation by dual ascent of the log-likelihood. *Communications in Mathematical Sciences*, 8(1):217–233, 2010. ISSN 15396746, 19450796. doi: 10.4310/CMS.2010.v8.n1.a11.
- Yee Whye Teh, Max Welling, Simon Osindero, and Geoffrey E Hinton. Energy-based models for sparse overcomplete representations. *Journal of Machine Learning Research*, 4(Dec):1235–1260, 2003.
- Benigno Uria, Marc-Alexandre Côté, Karol Gregor, Iain Murray, and Hugo Larochelle. Neural Autoregressive Distribution Estimation. *Journal of Machine Learning Research*, 17(205):1–37, 2016. ISSN 1533-7928.
- Rodrigo Veiga, Ludovic Stephan, Bruno Loureiro, Florent Krzakala, and Lenka Zdeborová. Phase diagram of stochastic gradient descent in high-dimensional two-layer neural networks, 2023.
- Dian Wu, Lei Wang, and Pan Zhang. Solving statistical mechanics using variational autoregressive networks. *Phys. Rev. Lett.*, 122:080602, Feb 2019. doi: 10.1103/PhysRevLett.122.080602. URL <https://link.aps.org/doi/10.1103/PhysRevLett.122.080602>.
- Ji Xu, Daniel J Hsu, and Arian Maleki. Global analysis of expectation maximization for mixtures of two gaussians. In D. Lee, M. Sugiyama, U. Luxburg, I. Guyon, and R. Garnett, editors, *Advances in Neural Information Processing Systems*, volume 29. Curran Associates, Inc., 2016. URL [https://proceedings.neurips.cc/paper\\_files/paper/2016/file/792c7b5aae4a79e78aaeda80516ae2ac-Paper.pdf](https://proceedings.neurips.cc/paper_files/paper/2016/file/792c7b5aae4a79e78aaeda80516ae2ac-Paper.pdf).

# Appendix

## A Derivation of summary statistics evolution

### A.1 Recap of the setting

For the reader convenience, we start by recalling the setting. We are interested in studying the following *variational inference* (VI) objective:

$$\mathcal{L}(\theta) := D_{\text{KL}}(q_\theta || p) = \mathbb{E}_{x \sim q_\theta} [\log q_\theta(x)] - \mathbb{E}_{x \sim q_\theta} [\log p(x)] \quad (23)$$

where the target distribution  $p(x)$  is given by a 2-Gaussian mixture model:

$$p(x) = w_\star \mathcal{N}(x | \mu_\star, I_d) + (1 - w_\star) \mathcal{N}(x | -\mu_\star, I_d), \quad (24)$$

with centroids  $\mu_\star \in \mathbb{R}^d$  having norm  $\|\mu_\star\|_2 = R$ . The variational family  $q_\theta$  is given by a K-Gaussian mixture:

$$q_\theta(x) = \sum_{i=1}^K w_i \mathcal{N}(x | \mu_i, I_d), \quad (25)$$

with  $K \geq 2$ , with both the centroids  $\mu_i \in \mathbb{R}^d$  and the weights  $w_i \in [0, 1]$  being trainable parameters. Therefore,  $\theta = \{(\mu_i, w_i) \in \mathbb{R}^d \times [0, 1] : i = 1, \dots, K\}$ . In particular, note that  $w_i$  need to be normalised:  $\sum_{i=1}^K w_i = 1$ .

For this setting, the loss function in eq. (23) can be explicitly written as

$$\mathcal{L}(\theta) = \sum_{i=1}^K w_i \mathbb{E}_{z \sim \mathcal{N}(0, I_d)} \left[ \log \sum_{j=1}^K w_j \mathcal{N}(z | \mu_j - \mu_i, I_d) - \log [w_\star \mathcal{N}(z | \mu_\star - \mu_i) + (1 - w_\star) \mathcal{N}(z | \mu_\star + \mu_i, I_d)] \right] \quad (26)$$

Noting that:

$$\mathcal{N}(z | \mu_j - \mu_i, I_d) = \frac{1}{(2\pi)^{d/2}} e^{-\frac{1}{2} \|z - (\mu_j - \mu_i)\|^2} = \frac{1}{(2\pi)^{d/2}} e^{-\frac{1}{2} \|z + \mu_i\|^2 + \mu_j^\top (z + \mu_i) - \frac{1}{2} \|\mu_j\|_2^2} \quad (27)$$

We can factor out  $\exp(-\|z + \mu_i\|^2/2)/(2\pi)^{d/2}$  through logarithm to simplify the loss:

$$\mathcal{L}(\theta) = \sum_{i=1}^K w_i \mathbb{E}_{z \sim \mathcal{N}(0, I_d)} \left[ \log \sum_{j=1}^K w_j e^{\mu_j^\top (z + \mu_i) - \frac{1}{2} \|\mu_j\|_2^2} - \log \left[ w_\star e^{\mu_\star^\top (z + \mu_i) - \frac{1}{2} \|\mu_\star\|_2^2} + (1 - w_\star) e^{-\mu_\star^\top (z + \mu_i) - \frac{1}{2} \|\mu_\star\|_2^2} \right] \right] \quad (28)$$

Note that since  $z \sim \mathcal{N}(0, I_d)$ , the loss function above only depends on the vectors  $\mu_c, \mu_\star$  through the following real-valued summary statistics:

$$R^2 = \|\mu_\star\|_2^2, \quad m_i = \frac{\mu_i^\top \mu_\star}{R^2}, \quad s_{ij} = \frac{\mu_i^\top \mu_j}{R^2}, \quad i, j = 1, \dots, K \quad (29)$$

This observation suggests that to characterize the landscape  $\mathcal{L}$ , it is enough to look at its dependence on these scalar variables. This is the key idea in the analysis that will follow. To alleviate the discussion, we will consider two simplifications in what follows:

1. First, we will focus the derivation to the case  $K = 2$ . The extension to  $K > 2$  is cumbersome but straightforward, and we will give the equations in Appendix A.5.1.
2. Second, we fix the norm of the variational models centroids to the target norm:  $\|\mu_i\|_2^2 = R$ . Under this assumption, the loss can be further simplified by factoring out  $\|\mu_j\|_2^2 = \|\mu_\star\|_2^2 = R^2$ :

$$\mathcal{L}(\theta) = \sum_{i=1}^K w_i \mathbb{E}_{z \sim \mathcal{N}(0, I_d)} \left[ \log \sum_{j=1}^K w_j e^{\mu_j^\top (z + \mu_i)} - \log \left[ w_\star e^{\mu_\star^\top (z + \mu_i)} + (1 - w_\star) e^{-\mu_\star^\top (z + \mu_i)} \right] \right] \quad (30)$$

In terms of the summary statistics, this implies that  $s_{ii} = 1$ . Although this assumption changes the optimization landscape, we empirically observe it has no important effect in the discussion of mode collapse, which is our main goal in this manuscript. For the sake of completeness, we discuss the unconstrained equations in Appendix A.5.2.

## A.2 Equations for the evolution of the means

We now discuss the derivation of eq. (8) for the evolution of the summary statistics under gradient flow. By definition, spherical gradient flow is given by:

$$\dot{\mu}_i = \nabla_{\mu_i}^{\mathbb{S}} \mathcal{L}(\mu_i, w_i) := \left( I_d - \frac{\mu_i \mu_i^\top}{R^2} \right) \nabla_{\mu_i} \mathcal{L}(\mu_i, w_i), \quad i = 1, 2. \quad (31)$$

First, let's compute the Euclidean gradient of the loss 30 with respect to  $\mu_{1,2}$ .

$$\begin{aligned} \nabla_{\mu_1} \mathcal{L} = & w_1 \mathbb{E}_{z \sim \mathcal{N}(0, I_d)} \left[ \frac{w_1(z + 2\mu_1)e^{\mu_1^\top(z + \mu_1)} + w_2\mu_2 e^{\mu_2^\top(z + \mu_1)}}{w_1 e^{\mu_1^\top(z + \mu_1)} + w_2 e^{\mu_2^\top(z + \mu_1)}} - \frac{\mu_\star w_\star e^{\mu_\star^\top(z + \mu_1)} - \mu_\star(1 - w_\star)e^{-\mu_\star^\top(z + \mu_1)}}{w_\star e^{\mu_\star^\top(z + \mu_1)} + (1 - w_\star)e^{-\mu_\star^\top(z + \mu_1)}} \right] \\ & + w_2 \mathbb{E}_{z \sim \mathcal{N}(0, I_d)} \left[ \frac{w_1(\mu_2 + z)e^{\mu_1^\top(z + \mu_2)}}{w_1 e^{\mu_1^\top(z + \mu_2)} + w_2 e^{\mu_2^\top(z + \mu_2)}} \right] \end{aligned} \quad (32)$$

Defining the sigmoid function  $\sigma(t) = (1 + e^{-t})^{-1}$ , we can re-rewrite:

$$\begin{aligned} \nabla_{\mu_1} \mathcal{L} = & w_1 \mathbb{E}_{z \sim \mathcal{N}(0, I_d)} \left[ (z + 2\mu_1) \sigma \left( (\mu_1 - \mu_2)^\top(z + \mu_1) + \log \frac{w_1}{w_2} \right) + \mu_2 \sigma \left( (\mu_2 - \mu_1)^\top(z + \mu_1) + \log \frac{w_2}{w_1} \right) \right. \\ & \left. + \mu_\star \left( 1 - 2\sigma \left( 2\mu_\star^\top(z + \mu_1) + \log \frac{w_\star}{1 - w_\star} \right) \right) \right] \\ & + w_2 \mathbb{E}_{z \sim \mathcal{N}(0, I_d)} \left[ (z + \mu_2) \sigma \left( (\mu_1 - \mu_2)^\top(z + \mu_2) + \log \frac{w_1}{w_2} \right) \right] \end{aligned} \quad (33)$$

It's convenient to eliminate  $zg(z)$ -like terms using Stein's lemma. Since  $z \sim \mathcal{N}(0, I_d)$ , we have  $\mathbb{E}_z[zg(z)] = \mathbb{E}_z[\nabla g(z)]$ , and:

$$\begin{aligned} \nabla_{\mu_1} \mathcal{L} = & w_1 \mathbb{E}_{z \sim \mathcal{N}(0, I_d)} \left[ \mu_1 \sigma \left( (\mu_1 - \mu_2)^\top(z + \mu_1) + \log \frac{w_1}{w_2} \right) \left( 3 - \sigma \left( (\mu_1 - \mu_2)^\top(z + \mu_1) + \log \frac{w_1}{w_2} \right) \right) \right. \\ & \left. + \mu_2 \sigma \left( (\mu_2 - \mu_1)^\top(z + \mu_1) + \log \frac{w_2}{w_1} \right)^2 + \mu_\star \left( 1 - 2\sigma \left( 2\mu_\star^\top(z + \mu_1) + \log \frac{w_\star}{1 - w_\star} \right) \right) \right] \\ & + w_2 \mathbb{E}_{z \sim \mathcal{N}(0, I_d)} \left[ \mu_1 \sigma \left( (\mu_1 - \mu_2)^\top(z + \mu_2) + \log \frac{w_1}{w_2} \right) \left( 1 - \sigma \left( (\mu_1 - \mu_2)^\top(z + \mu_2) + \log \frac{w_1}{w_2} \right) \right) \right. \\ & \left. + \mu_2 \sigma \left( (\mu_1 - \mu_2)^\top(z + \mu_2) + \log \frac{w_1}{w_2} \right)^2 \right] \end{aligned} \quad (34)$$

Projecting gradient on sphere with 6 results in

$$\begin{aligned} \nabla_{\mu_1}^{\mathbb{S}} \mathcal{L} = & (\mu_2 - \mu_1 s) \mathbb{E}_{z \sim \mathcal{N}(0, I_d)} \left[ w_1 \sigma \left( (\mu_2 - \mu_1)^\top(z + \mu_1) + \log \frac{w_2}{w_1} \right)^2 + w_2 \sigma \left( (\mu_1 - \mu_2)^\top(z + \mu_2) + \log \frac{w_1}{w_2} \right)^2 \right] \\ & + w_1 (\mu_\star - m_1 \mu_1) \mathbb{E}_{z \sim \mathcal{N}(0, I_d)} \left[ 1 - 2\sigma \left( 2\mu_\star^\top(z + \mu_1) + \log \frac{w_\star}{1 - w_\star} \right) \right] \end{aligned} \quad (35)$$

Introducing the following jointly Gaussian variables:

$$\lambda_\star = \frac{\mu_\star}{R} z, \quad \lambda = \frac{\mu_1 - \mu_2}{\sqrt{2R^2(1-s)}} z \quad (36)$$

we can rewrite:

$$\begin{aligned} \nabla_{\mu_1}^{\mathbb{S}} \mathcal{L} = & (\mu_2 - \mu_1 s) \mathbb{E}_{\lambda} \left[ w_1 \sigma \left( R^2(s-1) + \lambda R \sqrt{2(1-s)} + \log \frac{w_2}{w_1} \right)^2 + w_2 \sigma \left( R^2(s-1) + \lambda R \sqrt{2(1-s)} + \log \frac{w_1}{w_2} \right)^2 \right] \\ & + w_1 (\mu_{\star} - m_1 \mu_1) \mathbb{E}_{\lambda_{\star}} \left[ 1 - 2\sigma \left( 2R^2 m_1 + 2R \lambda_{\star} + \log \frac{w_{\star}}{1-w_{\star}} \right) \right] \end{aligned} \quad (37)$$

Introducing the following functions:

$$f(s) = \mathbb{E}_{\lambda} \left[ w_1 \sigma \left( R^2(s-1) + \lambda R \sqrt{2(1-s)} + \log \frac{w_2}{w_1} \right)^2 + w_2 \sigma \left( R^2(s-1) + \lambda R \sqrt{2(1-s)} + \log \frac{w_1}{w_2} \right)^2 \right] \quad (38)$$

$$g(m) = \mathbb{E}_{\lambda_{\star}} \left[ 1 - 2\sigma \left( 2R^2 m_1 + 2R \lambda_{\star} + \log \frac{w_{\star}}{1-w_{\star}} \right) \right] \quad (39)$$

We can conveniently write the spherical gradient as:

$$\nabla_{\mu_1}^{\mathbb{S}} \mathcal{L} = (\mu_2 - \mu_1 s) f(s) + w_1 (\mu_{\star} - m_1 \mu_1) g(m_1) \quad (40)$$

Using symmetry of loss  $\mu_1 \rightarrow \mu_2$ ,  $\mu_{\star} \rightarrow -\mu_{\star}$ ,  $w_1 \rightarrow w_2$ ,  $w_{\star} \rightarrow 1 - w_{\star}$  we obtain gradient with respect to  $\mu_2$

$$\nabla_{\mu_2}^{\mathbb{S}} \mathcal{L} = (\mu_1 - \mu_2 s) f(s) + w_2 (\mu_{\star} - m_2 \mu_2) g(m_2) \quad (41)$$

Finally, we compute the evolution of sufficient statistics by writing:

$$\begin{aligned} \dot{m}_{1,2} &= \frac{1}{R^2} \mu_{\star}^{\top} \dot{\mu}_{1,2} = -\frac{1}{R^2} \mu_{\star}^{\top} \nabla_{\mu_{1,2}}^{\mathbb{S}} \mathcal{L} \\ &= -[(m_{2,1} - m_{1,2} s) f(s) + w_{1,2} (1 - m_{1,2}^2) g(m_{1,2})] \end{aligned} \quad (42)$$

$$\begin{aligned} \dot{s} &= \frac{1}{R^2} \dot{\mu}_1^{\top} \mu_2 + \mu_1^{\top} \dot{m}_2 = -\frac{1}{R^2} [\mu_2^{\top} \nabla_{\mu_1}^{\mathbb{S}} \mathcal{L} + \mu_1^{\top} \nabla_{\mu_2}^{\mathbb{S}} \mathcal{L}] \\ &= -[2(1-s^2) f(s) + w_1 (m_2 - m_1 s) g(m_1) + w_2 (m_1 - m_2 s) g(m_2)] \end{aligned} \quad (43)$$

which are precisely the eq. (8) written in the main.

### A.3 Fixed points of the mean evolution

By definition, the fixed points of the flow eq. (8) are the zero gradient points. That is, we look for  $(m_1, m_2, s) \in [-1, 1]^3$  such that:

$$(m_2 - m_1 s) f(s) + w_1 (1 - m_1^2) g(m_1) = 0 \quad (44)$$

$$(m_1 - m_2 s) f(s) + w_2 (1 - m_2^2) g(m_2) = 0 \quad (45)$$

$$2(1-s^2) f(s) + w_1 (m_2 - m_1 s) g(m_1) + w_2 (m_1 - m_2 s) g(m_2) = 0 \quad (46)$$

First, suppose that  $1 - m_1^2 = 0$ . Then since  $f(s) > 0$  for any  $s$ , from eq. (44) we get  $m_2 - m_1 s = 0$ . Equation (45) simplifies to

$$m_1 (1 - s^2) f(s) + w_2 (1 - s^2) g(m_2) = 0 \quad (47)$$

Substituting into eq. (46) gives

$$2(1-s^2) f(s) + w_2 m_1 (1 - s^2) g(m_2) = 2(1-s^2) f(s) - m_1^2 (1 - s^2) f(s) = (1-s^2) f(s) = 0 \quad (48)$$

Again by positivity of  $f(s)$ ,  $s = \pm 1$ . By symmetry, if either  $m_1$  or  $m_2$  is  $\pm 1$ , then  $s = \pm 1$  and we have global minimum/flipped fixed point at  $s = -1$  or full alignment at  $s = 1$ .

Second, suppose that both  $m_{1,2} \in (-1, 1)$ , but  $g(m_1) = 0$ . Then eq. (44) implies  $m_2 - m_1 s = 0$  and eq. (46) simplifies to

$$2(1-s^2) f(s)^2 = w_2^2 (1 - m_1^2 s^2) m_1^2 (1 - s^2)^2 \frac{f(s)^2}{w_2^2 (1 - m_1^2 s^2)^2} \Rightarrow 2 = \frac{m_1^2 (1 - s^2)}{1 - m_1^2 s^2} \vee 1 - s^2 = 0 \quad (49)$$

The first equation results in the extremal solution  $m_1^2 = 1$ , which we have already considered. The second one gives  $s = \pm 1$ . If  $s = 1$ , then  $m_2 = m_1 = m$ , where  $g(m) = 0$ , which we check to be a full alignment fixed point. We would reach the same conclusion if we started from  $g(m_2) = 0$ .

Third, consider the general case when  $m_{1,2} \in (-1, 1)$  and  $g(m) \neq 0$ . Unfortunately, an explicit solution for the general fixed points is not available. Instead, we derive an unexpected geometrical connection between the three summary statistics.

Consider the  $3 \times 3$  matrix  $P$  formed by scalar products of means

$$P = \frac{1}{R^2} \begin{bmatrix} \mu_\star^\top \mu_\star & \mu_\star^\top \mu_1 & \mu_\star^\top \mu_2 \\ \mu_1^\top \mu_\star & \mu_1^\top \mu_1 & \mu_1^\top \mu_2 \\ \mu_2^\top \mu_\star & \mu_2^\top \mu_1 & \mu_2^\top \mu_2 \end{bmatrix} = \begin{bmatrix} 1 & m_1 & m_2 \\ m_1 & 1 & s \\ m_2 & s & 1 \end{bmatrix} \quad (50)$$

It is semidefinite positive because for any vector  $v \in \mathbb{R}^3$ ,

$$v^\top P v = \sum_{ij} v_i \mu_i^\top \mu_j v_j = \left( \sum_i v_i \mu_i \right)^\top \left( \sum_j v_j \mu_j \right) \geq 0 \quad (51)$$

Any semidefinite matrix has a non-negative determinant. Let us study how this condition evolves throughout the flow eq. (8) by writing:

$$\begin{aligned} \frac{d}{dt} \det P &= \frac{d}{dt} (1 + 2m_1 m_2 s - m_1^2 - m_2^2 - s^2) \\ &= 2 [\dot{m}_1 (m_2 s - m_1) + \dot{m}_2 (m_1 s - m_2) + \dot{s} (m_1 m_2 - s)] \\ &= 2(-1 + m_1^2 + m_2^2 - 2m_1 m_2 s + s^2) [2s f(s) + m_1 w_1 g(m_1) + m_2 w_2 g(m_2)] \\ &= -2 [2s f(s) + m_1 w_1 g(m_1) + m_2 w_2 g(m_2)] \det P \end{aligned} \quad (52)$$

At the fixed point, the time derivative of  $\det P$  is zero, meaning that either  $\det P = 0$  or the expression in the brackets vanishes. Let us start from the second case. Multiplying it by  $s$  and summing with eq. (46) we get:

$$2f(s) + w_1 m_2 g(m_1) + w_2 m_1 g(m_2) = 0 \quad (53)$$

We can substitute  $f(s)$  into eq. (44) and eq. (45) and rearrange terms to get:

$$w_1 g(m_1) (2 - 2m_1^2 - m_2^2 + m_1 m_2 s) = w_2 m_1 g(m_2) (m_2 - m_1 s) \quad (54)$$

$$w_2 g(m_2) (2 - 2m_2^2 - m_1^2 + m_1 m_2 s) = w_1 m_2 g(m_1) (m_1 - m_2 s) \quad (55)$$

Since we have assumed earlier that  $g(m_1) \neq 0$  and  $g(m_2) \neq 0$  we can combine these expressions into:

$$m_1 (m_2 - m_1 s) (2 - 2m_2^2 - m_1^2 + m_1 m_2 s) = m_2 (m_1 - m_2 s) (2 - 2m_1^2 - m_2^2 + m_1 m_2 s) \quad (56)$$

Since again  $g(m_1) \neq 0$ ,  $1 - m_1^2 \neq 0$ ,  $f(s) > 0$ ,  $m_2 - m_1 s \neq 0$  and by analogy  $m_1 - m_2 s \neq 0$ . Since the weights are unbalanced we can't have  $m_{1,2} = 0$  either, so the only possibility is that  $2 - 2m_2^2 - m_1^2 + m_1 m_2 s = 2 - 2m_1^2 - m_2^2 + m_1 m_2 s = 0$ , implying that  $\det P$  equal to half sum of these terms is also zero. Therefore, in both the first and second cases:

$$\det P = 1 + 2m_1 m_2 s - m_1^2 - m_2^2 - s^2 = 0 \Rightarrow s = m_1 m_2 \pm \sqrt{(1 - m_1^2)(1 - m_2^2)} \quad (57)$$

This interesting geometrical constraint can be used to restrict the space of possible fixed points.

**Hessian calculation** To investigate the stability of the fixed points we need to linearize the flow equations eq. (8) around them. The linear system is written as

$$\frac{d}{dt} \begin{bmatrix} \delta m_1 \\ \delta m_2 \\ \delta s \end{bmatrix} = -H \begin{bmatrix} \delta m_1 \\ \delta m_2 \\ \delta s \end{bmatrix} \quad (58)$$

where we call  $H$  as Hessian at the fixed point.

First, when  $m_1 = \pm 1$  and  $s = \pm 1$ ,  $m_2 - m_1 s$  and  $1 - m_1^2$  terms vanish and we can discard terms containing derivatives of  $f$  and  $g$  arising during linearization

$$\delta \dot{m}_1 = - \left[ (\delta m_2 - s \delta m_1 - m_1 \delta s) f(s) - \frac{2\gamma m_1}{\gamma + 1} g(m_1) \delta m_1 \right] \quad (59)$$

$$\delta \dot{m}_2 = - \left[ (\delta m_1 - s \delta m_2 - m_2 \delta s) f(s) - \frac{2m_2}{\gamma + 1} g(m_2) \delta m_2 \right] \quad (60)$$

$$\delta \dot{s} = - \left[ -4s f(s) \delta s + \frac{\gamma}{\gamma + 1} g(m_1) (\delta m_2 - s \delta m_1 - m_1 \delta s) + \frac{1}{\gamma + 1} g(m_2) (\delta m_1 - s \delta m_2 - m_2 \delta s) \right] \quad (61)$$

Eigenvalues of  $H$  at global minimum  $(m_1^*, m_2^*, s^*) = (1, -1, -1)$  are

$$\lambda = 2f(-1) - w_1 g(1) + w_2 g(-1) \quad (62)$$

$$\lambda_{\pm} = 2f(-1) - w_1 g(1) + w_2 g(-1) \pm \sqrt{4f(-1)^2 + (w_1 g(1) + w_2 g(-1))^2} \quad (63)$$

At flipped fixed point  $(m_1^*, m_2^*, s^*) = (-1, 1, -1)$  they are

$$\lambda = 2f(-1) - w_2 g(1) + w_1 g(-1) \quad (64)$$

$$\lambda_{\pm} = 2f(-1) - w_2 g(1) + w_1 g(-1) \pm \sqrt{4f(-1)^2 + (w_2 g(1) + w_1 g(-1))^2} \quad (65)$$

At perfect alignment mode collapse fixed point  $(m_1^*, m_2^*, s^*) = (1, 1, 1)$  they are

$$\lambda = -2f(1) - g(1) \quad (66)$$

$$\lambda_{\pm} = -2f(1) - g(1) \pm \sqrt{4f(1)^2 + \frac{(1 - w_2)^2}{(1 + w_2)^2} g(1)^2} \quad (67)$$

At opposite fixed point  $(m_1^*, m_2^*, s^*) = (-1, -1, 1)$  they are

$$\lambda = -2f(1) + g(-1) \quad (68)$$

$$\lambda_{\pm} = -2f(1) + g(-1) \pm \sqrt{4f(1)^2 + \frac{(1 - w_2)^2}{(1 + w_2)^2} g(-1)^2} \quad (69)$$

For the last perfect alignment fixed point,  $m_2 = m_1 = m$ , where  $g(m) = 0$  and  $s = 1$ . Then  $m_2 - m_1 s$  vanishes and linearized equations are

$$\delta \dot{m}_1 = - \left[ (\delta m_2 - s \delta m_1 - m_1 \delta s) f(s) + \frac{\gamma}{\gamma + 1} (1 - m_1^2) g'(m_1) \delta m_1 \right] \quad (70)$$

$$\delta \dot{m}_2 = - \left[ (\delta m_1 - s \delta m_2 - m_2 \delta s) f(s) + \frac{1}{\gamma + 1} (1 - m_2^2) g'(m_2) \delta m_2 \right] \quad (71)$$

$$\delta \dot{s} = 4s f(s) \delta s \quad (72)$$

Eigenvalues of  $H$  are

$$\lambda = -4f(1) \quad (73)$$

$$\lambda_{\pm} = w_1 (1 - m^2) g'(m) - 1 \pm \sqrt{f(1)^2 + \frac{1}{4} w_1^2 (1 - m^2)^2 g'(m)^2} \quad (74)$$

For any  $w_{1,2}$  and  $R$ , the point is unstable due to  $\lambda < 0$ , which is expected. For other points above we numerically confirm that perfect alignment fixed points are unstable, global minimum is stable, and flipped fixed point is stable for large enough  $R$  and is unstable otherwise.

## A.4 Weights evolution

We now turn our attention to the evolution of the weights  $w_1, w_2 \in [0, 1]$ . Note that the naive flow  $\dot{w}_i = \nabla_{w_i} \mathcal{L}(\theta)$  does not respect the normalization constraint  $w_1 + w_2 = 1$ , and therefore take us out of the space of probability density functions. Different solutions for this can be considered, each leading to a different VI algorithm with different optimization properties. Here, we consider two particular solutions: a *reparametrized flow* and a *projected flow*, which we discuss below. In both cases, the key idea is to see the flow as the vanishing step-size limit of a gradient descent algorithm that preserves the weights.

### A.4.1 Reparametrized flow

The first idea consists of enforcing the normalisation by considering the following reparametrization of the weights:

$$w_1 = \frac{v_1}{v_1 + v_2}, \quad w_2 = \frac{v_2}{v_1 + v_2}; \quad (75)$$

where  $v_1, v_2 \in \mathbb{R}_+$ . This can be implemented via the following gradient descent scheme:

1. Initialize differentiable parameters  $v_1 = w_1, v_2 = w_2$
2. Parameterize weights as

$$w_1 = \frac{v_1}{v_1 + v_2}; \quad w_2 = \frac{v_2}{v_1 + v_2}; \quad (76)$$

3. Update parameters with gradient descent

$$v'_1 = v_1 - \eta \frac{\partial \mathcal{L}(w_1, w_2)}{\partial v_1}; \quad v'_2 = v_2 - \eta \frac{\partial \mathcal{L}(w_1, w_2)}{\partial v_2}; \quad (77)$$

Here  $w_{1,2}$  are functions of  $v_{1,2}$  according to 76.

4. Obtain new weights with parameterization eq. (76).

$$w'_1 = \frac{v'_1}{v'_1 + v'_2}; \quad w'_2 = \frac{v'_2}{v'_1 + v'_2}; \quad (78)$$

Thus, we have explicitly preserved normalization constraint at the end of each iteration.

It is easy to see that this gradient descent scheme preserve the normalization  $w_1 + w_2 = 1$ . To implement the above, we need to compute the gradients in  $v_1, v_2$ . First, consider the gradient of the loss with respect to  $v_1$ , it is given by:

$$\begin{aligned} \frac{\partial \mathcal{L}}{\partial v_1} &= \frac{\partial \mathcal{L}}{\partial w_1} \frac{\partial w_1}{\partial v_1} + \frac{\partial \mathcal{L}}{\partial w_2} \frac{\partial w_2}{\partial v_1} = \frac{v_2}{(v_1 + v_2)^2} \frac{\partial \mathcal{L}}{\partial w_1} - \frac{v_2}{(v_1 + v_2)^2} \frac{\partial \mathcal{L}}{\partial w_2} \\ &= w_2 \left( \frac{\partial \mathcal{L}}{\partial w_1} - \frac{\partial \mathcal{L}}{\partial w_2} \right) \end{aligned} \quad (79)$$

Similarly, by symmetry the gradient of the loss with respect to  $v_2$  is given by:

$$\frac{\partial \mathcal{L}}{\partial v_2} = w_1 \left( \frac{\partial \mathcal{L}}{\partial w_2} - \frac{\partial \mathcal{L}}{\partial w_1} \right) \quad (80)$$

Therefore, gradient descent update (step 4, eq. (78)) is given by:

$$w'_1 = w_1 - \eta \left[ v_2 \frac{\partial \mathcal{L}}{\partial v_1} - v_1 \frac{\partial \mathcal{L}}{\partial v_2} \right] + O(\eta^2) \quad (81)$$

$$= w_1 - \eta(w_1^2 + w_2^2) \left( \frac{\partial \mathcal{L}}{\partial w_1} - \frac{\partial \mathcal{L}}{\partial w_2} \right) + O(\eta^2) \quad (82)$$

And hence the limiting  $\eta \rightarrow 0^+$  flow is:

$$\dot{w}_1 = -(w_1^2 + w_2^2) \left( \frac{\partial \mathcal{L}}{\partial w_1} - \frac{\partial \mathcal{L}}{\partial w_2} \right) \quad (83)$$

$$\dot{w}_2 = -\dot{w}_1 \quad (84)$$

Finally, it remains to show that the equations above can be written in terms of the summary statistics  $(m_1, m_2, s)$ . For that, we need to compute the gradients of the loss with respect to the weights  $(w_1, w_2)$ . Starting from  $w_1$ :

$$\begin{aligned} \frac{\partial \mathcal{L}}{\partial w_1} &= \mathbb{E}_{z \sim \mathcal{N}(0, I_d)} \left[ \frac{w_1 e^{\mu_1^\top (z + \mu_1)}}{w_1 e^{\mu_1^\top (z + \mu_1)} + w_2 e^{\mu_2^\top (z + \mu_1)}} + \frac{w_2 e^{\mu_1^\top (z + \mu_2)}}{w_1 e^{\mu_1^\top (z + \mu_2)} + w_2 e^{\mu_2^\top (z + \mu_2)}} \right] \\ &\quad + \mathbb{E}_{z \sim \mathcal{N}(0, I_d)} \left[ \log \left( w_1 e^{\mu_1^\top (z + \mu_1)} + w_2 e^{\mu_2^\top (z + \mu_1)} \right) - \log \left( w_\star e^{\mu_\star^\top (z + \mu_1)} + (1 - w_\star) e^{-\mu_\star^\top (z + \mu_1)} \right) \right] \end{aligned} \quad (85)$$

$$\begin{aligned} &= \mathbb{E}_{z \sim \mathcal{N}(0, I_d)} \left[ \sigma \left( \mu_1^\top (\mu_1 - \mu_2) + (\mu_1 - \mu_2)^\top z + \log \frac{w_1}{w_2} \right) + \frac{w_2}{w_1} \sigma \left( \mu_2^\top (\mu_1 - \mu_2) + (\mu_1 - \mu_2)^\top z + \log \frac{w_1}{w_2} \right) \right] \\ &\quad + \mathbb{E}_{z \sim \mathcal{N}(0, I_d)} \left[ \log \frac{w_1}{w_\star} + \mu_1^\top (z + \mu_1) - \mu_\star^\top (z + \mu_1) - \log \sigma \left( (\mu_1 - \mu_2)^\top (z + \mu_1) + \log \frac{w_1}{w_2} \right) \right] \\ &\quad + \mathbb{E}_{z \sim \mathcal{N}(0, I_d)} \left[ \log \sigma \left( 2\mu_\star^\top (z + \mu_1) + \log \frac{w_\star}{1 - w_\star} \right) \right] \end{aligned} \quad (86)$$

As in Appendix A.2, we now introduce the jointly Gaussian random variables:

$$\lambda = \frac{\mu_1 - \mu_2}{\sqrt{2R^2(1-s)}} z, \quad \lambda_\star = \frac{\mu_\star}{R} z. \quad (87)$$

Introduce sufficient statistics and rewrite:

$$\begin{aligned} \frac{\partial \mathcal{L}}{\partial w_1} &= \mathbb{E}_\lambda \left[ \sigma \left( R^2(1-s) + \lambda R \sqrt{2(1-s)} + \log \frac{w_1}{w_2} \right) + \frac{w_2}{w_1} \sigma \left( -R^2(1-s) + \lambda R \sqrt{2(1-s)} + \log \frac{w_1}{w_2} \right) \right] \\ &\quad - \mathbb{E}_{\lambda, \lambda_\star} \left[ \log \sigma \left( R^2(1-s) + \lambda R \sqrt{2(1-s)} + \log \frac{w_1}{w_2} \right) + \log \sigma \left( 2R^2 m_1 + 2R \lambda_\star + \log \frac{w_\star}{1 - w_\star} \right) \right] \\ &\quad + \log \frac{w_1}{w_\star} + R^2(1 - m_1) \end{aligned} \quad (88)$$

We can obtain derivative  $\partial \mathcal{L} / \partial w_2$  in analogy by exploiting symmetry of loss under  $\mu_1 \rightarrow \mu_2$ ,  $\mu_\star \rightarrow -\mu_\star$ ,  $w_1 \rightarrow 1 - w_1 = w_2$ ,  $w_\star \rightarrow 1 - w_\star$ , which acts on statistics as  $m_1 \rightarrow -m_2$ ,  $s \rightarrow s$ ,  $\lambda \rightarrow -\lambda$  and  $\lambda_\star \rightarrow -\lambda_\star$ . We obtain

$$\begin{aligned} \frac{\partial \mathcal{L}}{\partial w_2} &= \mathbb{E}_\lambda \left[ \sigma \left( R^2(1-s) - \lambda R \sqrt{2(1-s)} - \log \frac{w_1}{w_2} \right) + \frac{w_1}{w_2} \sigma \left( -R^2(1-s) - \lambda R \sqrt{2(1-s)} - \log \frac{w_1}{w_2} \right) \right] \\ &\quad - \mathbb{E}_{\lambda, \lambda_\star} \left[ \log \sigma \left( R^2(1-s) - \lambda R \sqrt{2(1-s)} - \log \frac{w_1}{w_2} \right) + \log \sigma \left( -2R^2 m_2 - 2R \lambda_\star - \log \frac{w_\star}{1 - w_\star} \right) \right] \\ &\quad + \log \frac{w_2}{1 - w_\star} + R^2(1 + m_2) \end{aligned} \quad (89)$$

Together with eq. (83), this shows that the flow of the weights can be written in terms of  $(w_1, w_2, m_1, m_2, s)$ .

#### A.4.2 Projected gradient

An alternative approach to reparametrizing the variables consist of projecting the gradient on the weights back in the constraint set, similar to the spherical flow for the means. This can be implemented as follows:

1. At every step, we take a standard gradient descent on the weights:

$$w'_1 = w_1 - \eta \frac{\partial \mathcal{L}}{\partial w_1}; \quad w'_2 = w_2 - \eta \frac{\partial \mathcal{L}}{\partial w_2}; \quad (90)$$

2. Next, we normalize the weights such that  $w_1 + w_2 = 1$ :

$$w_1'' = \frac{w_1'}{w_1' + w_2'}; \quad w_2'' = \frac{w_2'}{w_1' + w_2'}; \quad (91)$$

To evaluate the update, we need to compute:

$$\begin{aligned} w_1'' &= \frac{w_1 - \eta \partial \mathcal{L} / \partial w_1}{w_1 - \eta \partial \mathcal{L} / \partial w_1 + w_2 - \eta \partial \mathcal{L} / \partial w_2} \\ &= \left( w_1 - \eta \frac{\partial \mathcal{L}}{\partial w_1} \right) \left( 1 + \eta \frac{\partial \mathcal{L}}{\partial w_1} + \eta \frac{\partial \mathcal{L}}{\partial w_2} \right) + O(\eta^2) \\ &= w_1 - \eta \left[ (1 - w_1) \frac{\partial \mathcal{L}}{\partial w_1} - w_1 \frac{\partial \mathcal{L}}{\partial w_2} \right] + O(\eta^2) \end{aligned} \quad (92)$$

$$= w_1 - \eta \left[ w_2 \frac{\partial \mathcal{L}}{\partial w_1} - w_1 \frac{\partial \mathcal{L}}{\partial w_2} \right] + O(\eta^2) \quad (93)$$

where in the second equality we expanded in small  $\eta \ll 1$ , keeping only the first order terms. Therefore, if we want a gradient flow to mimic the projected gradient, we have to compute  $w_2 \partial \mathcal{L} / \partial w_1 - w_1 \partial \mathcal{L} / \partial w_2$  instead of  $\partial \mathcal{L} / \partial w_1$ . Together with the symmetric expression for  $w_2''$  and the gradient of the weights previously derived in eq. (88) and eq. (89), this allows to write the projected flow in terms of the summary statistics.

However, we find that in comparison with the reparametrized flow from appendix A.4.1, this projected flow is more prompt to mode collapse with one of the weights going quickly to zero, in particular at small  $R$ . Let us consider limit  $R \rightarrow 0^+$  and compute the gradients in eq. (88) and eq. (89) up to second order of  $R$ :

$$\begin{aligned} \frac{\partial \mathcal{L}}{\partial w_1} &= \mathbb{E}_\lambda \left[ w_1 + w_1 w_2 \lambda R \sqrt{2(1-s)} + (1-s) w_1 w_2 (w_1(1-\lambda^2) + w_2(1+\lambda^2)) R^2 \right] \\ &\quad + \mathbb{E}_\lambda \left[ w_2 + w_2^2 \lambda R \sqrt{2(1-s)} - (1-s) w_2^2 (w_1(1+\lambda^2) + w_2(1-\lambda^2)) R^2 \right] \\ &\quad - \mathbb{E}_{\lambda, \lambda_*} \left[ \log w_1 + w_2 \lambda R \sqrt{2(1-s)} + (1-s) w_2 (w_2 + w_1(1-\lambda^2)) R^2 \right] \\ &\quad + \mathbb{E}_{\lambda, \lambda_*} \left[ \log w_* + 2\lambda R(1-w_*) - 2(1-w_*)(w_* \lambda^2 - m_1) R^2 \right] \\ &\quad + \log \frac{w_1}{w_*} + R^2(1-m_1^2) + o(R^2) \end{aligned} \quad (94)$$

After averaging out and using symmetry we get  $\partial \mathcal{L} / \partial w_{1,2}$

$$\frac{\partial \mathcal{L}}{\partial w_1} = 1 + R^2((1-m_1) - (1-s)w_2^2 + 2(1-w_*)(m_1 - w_*)) \quad (95)$$

$$\frac{\partial \mathcal{L}}{\partial w_2} = 1 + R^2((1+m_2) - (1-s)w_1^2 + 2w_*(-m_2 - 1 + w_*)) \quad (96)$$

At the gradient flow level, at  $R \rightarrow 0^+$ ,  $w_1$  evolves as:

$$\dot{w}_1 = - \left( w_2 \frac{\partial l}{\partial w_1} - w_1 \frac{\partial l}{\partial w_2} \right) = -(1 - w_1 - w_1) = 2(w_1 - 1/2) \quad (97)$$

The flow is linear and has an unstable expansion factor 2. A non-zero radius gives a  $O(R^2)$  correction which is insufficient to make the flow stable up until a certain radius threshold. Thus,  $w_1$  is just shot into 0 or 1, depending on initialization.

## A.5 Generalizations

In this section, we briefly discuss the generalization of the flow equations derived in Appendix A.2 to more general cases.

### A.5.1 General K-Gaussian mixture

Let us start with loss 28, use that  $\|\mu_\star\|^2 = R^2$  to simplify exponents and rewrite summation index  $i \rightarrow k$  to obtain

$$\mathcal{L}(\theta) = \sum_{k=1}^K w_k \mathbb{E}_{z \sim \mathcal{N}(0, I_d)} \left[ \log \sum_{j=1}^K w_j e^{\mu_j^\top (z + \mu_k) + \frac{1}{2}(R^2 - \|\mu_j\|_2^2)} - \log \left[ w_\star e^{\mu_\star^\top (z + \mu_k)} + (1 - w_\star) e^{-\mu_\star^\top (z + \mu_k)} \right] \right] \quad (98)$$

The gradient with respect to mean  $\mu_i$  is then

$$\begin{aligned} \nabla_{\mu_i} \mathcal{L} &= \sum_{k=1}^K w_k \mathbb{E}_z \frac{\sum_{j=1}^K w_j [(z + \mu_k - \mu_j) \delta_{ij} + \mu_j \delta_{ik}] e^{\mu_j^\top (z + \mu_k) + \frac{1}{2}(R^2 - \|\mu_j\|_2^2)}}{\sum_{j=1}^K w_j e^{\mu_j^\top (z + \mu_k) + \frac{1}{2}(R^2 - \|\mu_j\|_2^2)}} + \\ &w_i \mathbb{E}_z \mu_\star \left( 1 - 2\sigma \left( 2\mu_\star^\top (z + \mu_i) \log \frac{w_\star}{1 - w_\star} \right) \right) = \\ &\sum_{k=1}^K w_k \mathbb{E}_z \frac{w_i (z + \mu_k - \mu_i) e^{\mu_i^\top (z + \mu_k) + \frac{1}{2}(R^2 - \|\mu_i\|_2^2)}}{\sum_{j=1}^K w_j e^{\mu_j^\top (z + \mu_k) + \frac{1}{2}(R^2 - \|\mu_j\|_2^2)}} + w_i \mathbb{E}_z \frac{\sum_{j=1}^K w_j \mu_j e^{\mu_j^\top (z + \mu_i) + \frac{1}{2}(R^2 - \|\mu_j\|_2^2)}}{\sum_{j=1}^K w_j e^{\mu_j^\top (z + \mu_i) + \frac{1}{2}(R^2 - \|\mu_j\|_2^2)}} + \\ &w_i \mathbb{E}_z \mu_\star \left( 1 - 2\sigma \left( 2\mu_\star^\top (z + \mu_i) + \log \frac{w_\star}{1 - w_\star} \right) \right) \end{aligned} \quad (99)$$

Eliminate  $zg(z)$ -like terms with Stein's lemma

$$\begin{aligned} \nabla_{\mu_i} \mathcal{L} &= \sum_{k=1}^K w_k \mathbb{E}_z \frac{w_i (\mu_k - \mu_i) e^{\mu_i^\top (z + \mu_k) + \frac{1}{2}(R^2 - \|\mu_i\|_2^2)}}{\sum_{j=1}^K w_j e^{\mu_j^\top (z + \mu_k) + \frac{1}{2}(R^2 - \|\mu_j\|_2^2)}} + w_i \mu_i \sum_{k=1}^K w_k \mathbb{E}_z \frac{e^{\mu_i^\top (z + \mu_k) + \frac{1}{2}(R^2 - \|\mu_i\|_2^2)}}{\sum_{j=1}^K w_j e^{\mu_j^\top (z + \mu_k) + \frac{1}{2}(R^2 - \|\mu_j\|_2^2)}} \\ &- w_i \sum_{k=1}^K w_k \mathbb{E}_z \frac{e^{\mu_i^\top (z + \mu_k) + \frac{1}{2}(R^2 - \|\mu_i\|_2^2)} \sum_{j=1}^K w_j \mu_j e^{\mu_j^\top (z + \mu_k) + \frac{1}{2}(R^2 - \|\mu_j\|_2^2)}}{\left( \sum_{j=1}^K w_j e^{\mu_j^\top (z + \mu_k) + \frac{1}{2}(R^2 - \|\mu_j\|_2^2)} \right)^2} \\ &+ w_i \mathbb{E}_z \frac{\sum_{j=1}^K w_j \mu_j e^{\mu_j^\top (z + \mu_i) + \frac{1}{2}(R^2 - \|\mu_j\|_2^2)}}{\sum_{j=1}^K w_j e^{\mu_j^\top (z + \mu_i) + \frac{1}{2}(R^2 - \|\mu_j\|_2^2)}} + w_i \mathbb{E}_z \mu_\star \left( 1 - 2\sigma \left( 2\mu_\star^\top (z + \mu_i) + \log \frac{w_\star}{1 - w_\star} \right) \right) \end{aligned} \quad (100)$$

### A.5.2 Euclidean flow

Let's compute the Euclidean gradient of the loss eq. (98) when  $K = 2$

$$\begin{aligned} \nabla_{\mu_1} \mathcal{L} &= w_1 \mathbb{E}_z \frac{w_1 (z + \mu_1) e^{\mu_1^\top (z + \mu_1) + \frac{1}{2}(R^2 - \|\mu_1\|_2^2)} + w_2 \mu_2 e^{\mu_2^\top (z + \mu_1) + \frac{1}{2}(R^2 - \|\mu_2\|_2^2)}}{w_1 e^{\mu_1^\top (z + \mu_1) + \frac{1}{2}(R^2 - \|\mu_1\|_2^2)} + w_2 e^{\mu_2^\top (z + \mu_1) + \frac{1}{2}(R^2 - \|\mu_2\|_2^2)}} - \\ &w_1 \mathbb{E}_z \frac{\mu_\star w_\star e^{\mu_\star^\top (z + \mu_1)} - \mu_\star (1 - w_\star) e^{-\mu_\star^\top (z + \mu_1)}}{w_\star e^{\mu_\star^\top (z + \mu_1)} + (1 - w_\star) e^{-\mu_\star^\top (z + \mu_1)}} + \\ &w_2 \mathbb{E}_z \left[ \frac{w_1 (z + \mu_2 - \mu_1) e^{\mu_1^\top (z + \mu_2) + \frac{1}{2}(R^2 - \|\mu_1\|_2^2)}}{w_1 e^{\mu_1^\top (z + \mu_2) + \frac{1}{2}(R^2 - \|\mu_1\|_2^2)} + w_2 e^{\mu_2^\top (z + \mu_2) + \frac{1}{2}(R^2 - \|\mu_2\|_2^2)}} \right] \end{aligned} \quad (101)$$

Rewrite with sigmoid function as

$$\begin{aligned} \nabla_{\mu_1} \mathcal{L} &= w_1 \mathbb{E}_z \left[ (z + \mu_1) \sigma \left( (\mu_1 - \mu_2)^\top (z + \mu_1) + \frac{1}{2}(\|\mu_2\|_2^2 - \|\mu_1\|_2^2) + \log \frac{w_1}{w_2} \right) \right. \\ &+ \mu_2 \sigma \left( (\mu_2 - \mu_1)^\top (z + \mu_1) + \frac{1}{2}(\|\mu_1\|_2^2 - \|\mu_2\|_2^2) + \log \frac{w_2}{w_1} \right) \\ &+ \mu_\star \left( 1 - 2\sigma \left( 2\mu_\star^\top (z + \mu_1) + \log \frac{w_\star}{1 - w_\star} \right) \right) \Big] \\ &+ w_2 \mathbb{E}_z \left[ (z + \mu_2 - \mu_1) \sigma \left( (\mu_1 - \mu_2)^\top (z + \mu_2) + \frac{1}{2}(\|\mu_2\|_2^2 - \|\mu_1\|_2^2) + \log \frac{w_1}{w_2} \right) \right] \end{aligned} \quad (102)$$

Eliminate  $zg(z)$ -like terms with Stein’s lemma

$$\begin{aligned}
\nabla_{\mu_1} \mathcal{L} = & w_1 \mathbb{E}_z \left[ \mu_1 \sigma \left( (\mu_1 - \mu_2)^\top (z + \mu_1) + \frac{1}{2} (\|\mu_2\|_2^2 - \|\mu_1\|_2^2) + \log \frac{w_1}{w_2} \right) \right. \\
& \left( 2 - \sigma \left( (\mu_1 - \mu_2)^\top (z + \mu_1) + \frac{1}{2} (\|\mu_2\|_2^2 - \|\mu_1\|_2^2) + \log \frac{w_1}{w_2} \right) \right) \\
& + \mu_2 \sigma \left( (\mu_2 - \mu_1)^\top (z + \mu_1) + \frac{1}{2} (\|\mu_1\|_2^2 - \|\mu_2\|_2^2) + \log \frac{w_2}{w_1} \right)^2 \\
& + \mu_\star \left( 1 - 2\sigma \left( 2\mu_\star^\top (z + \mu_1) + \log \frac{w_\star}{1 - w_\star} \right) \right) \Big] \\
& + w_2 \mathbb{E}_z \left[ (\mu_2 - \mu_1) \sigma \left( (\mu_1 - \mu_2)^\top (z + \mu_2) + \frac{1}{2} (\|\mu_2\|_2^2 - \|\mu_1\|_2^2) + \log \frac{w_1}{w_2} \right)^2 \right] \quad (103)
\end{aligned}$$

## B Numerical experiments settings

### B.1 Normalizing flows

**RealNVPs** — One of the ways to construct expressive but invertible functions  $f_\theta$  is called RealNVP [Dinh et al., 2017]. The idea is compose coupling layers. These elementary operations partition coordinates of  $x$  using a binary mask  $b$  of the same dimension and then perform coordinate-wise translation and scaling with functions  $t : \mathbb{R}^d \rightarrow \mathbb{R}^d$  and  $s : \mathbb{R}^d \rightarrow \mathbb{R}^d$ , respectively. The transformation and its reverse is

$$y = bx + (1 - b) \left[ x \odot e^{s(bx)} + t(bx) \right] \quad (104)$$

$$x = by + (1 - b) [y - t(by)] \odot e^{-s(by)} \quad (105)$$

We can then stack several layers of such transformations and remain within the class of invertible functions.

**Monte Carlo estimators of gradients** — Considering the variational family of a normalizing flow with base distribution  $p_z$  and map  $f_\theta$ , the VI objective for a target with density  $p$  is the reverse KL:

$$\begin{aligned}
\mathcal{L}(\theta) &= D_{\text{KL}}(q_\theta \| p) = \mathbb{E}_{x \sim q_\theta} \log \frac{q_\theta(x)}{p(x)} \\
&= \mathbb{E}_{z \sim p_z} \left[ \log p_z(z) - \log |\nabla_z f_\theta(z)| - \log p(f_\theta(z)) \right], \quad (106)
\end{aligned}$$

where we have applied in the last line the “reparametrization trick”, viewing the VI loss as an expectation over the base density  $p_z$  instead of the flow density  $q_\theta$ . Since the distribution  $p_z$  doesn’t depend on  $\theta$ , we can calculate empirical gradients by sampling a batch of  $z$  of size  $B$  and then taking the gradient of an average of an expression in the square brackets.

**Hyperparameters** — In the experiments presented in section 4, we use RealNVPs with 6 coupling layers. The scaling network  $s$  and translation network  $t$  are multi-layer perceptrons with 3 hidden layers and hidden dimension  $h = 16$ . We fix  $w_1 = 2/3$ ,  $w_2 = 1/3$ , batch size  $B = 128$ . We perform optimization with Adam at a learning rate of  $10^{-3}$ . Training were considered converged when loss  $\mathcal{L}$  as well as the statistics  $\mu_\pm$  and  $w_\pm$  were stabilized in the course of 500 iterations, the number of iterations was roughly 1000-4000, depending on the input dimension  $d$

### B.2 Mixture of Gaussians

For the experiments considering the variational family of mixtures of bimodal Gaussians with consider the same batchsize  $B = 128$  and perform optimization with Adam at a learning rate of  $10^{-3}$ . Training were considered converged when statistics  $m_{1,2}$ ,  $s$ , and  $w_{1,2}$  were stable in the course of 200 iterations, the number of iterations was roughly 1000.